AD-A032 471 IOWA INST OF HYDRAULIC RESEARCH IOWA CITY F/G 13/2
A LABORATORY INVESTIGATION OF THE MECHANICS AND HYDRAULICS OF R--ETC(U)
MAR 76 J C TATINCLAUX, C L LEE, T P WANG DAAK03-75-C-0030
UNCLASSIFIED IIHR-186 NL

1 OF 2
AD-A
032 471

A LABORATORY INVESTIGATION OF THE MECHANICS AND HYDRAULICS OF RIVER ICE JAMS

Iowa Institute of Hydraulic Research
Iowa City, Iowa

March 1976

A LABORATORY INVESTIGATION OF THE MECHANICS AND HYDRAULICS OF RIVER ICE JAMS

by

J. C. Tatinclaux, C. L. Lee, T. P. Wang, T. Nakato,
and J. F. Kennedy

Sponsored by

U.S. Army Corps of Engineers Cold Regions Research and Engineering Laboratory, and U.S. Army Natick Laboratories
Contract No. DAAK03-75-C-0030

and

National Science Foundation
Grant No. ENG-72-04118A02

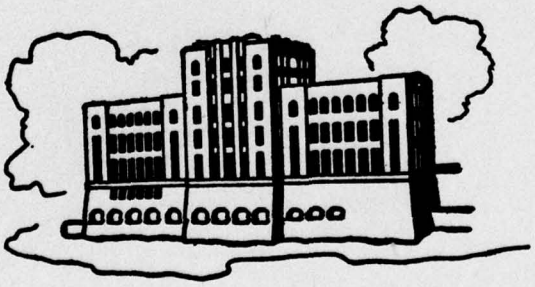

IIHR Report No. 186

Iowa Institute of Hydraulic Research
The University of Iowa
Iowa City, Iowa

March 1976

BIBLIOGRAPHIC DATA SHEET	1. Report No. UIIHR 186	2.	3. Recipient's Accession No.
4. Title and Subtitle A Laboratory Investigation of the Mechanics and Hydraulics of River Ice Jams			5. Report Date March 1976 6.
7. Author(s) J. C. Tatinclaux, C. L. Lee, T. P. Wang, T. Nakato, and J. F. Kennedy			8. Performing Organization Rept. No.
9. Performing Organization Name and Address Iowa Institute of Hydraulic Research The University of Iowa Iowa City, Iowa 52242			10. Project/Task/Work Unit No. 11. Contract/Grant No. DAAK03-75-C-0030 (NSF) ENG-72-04118A02
12. Sponsoring Organization Name and Address U. S. Army Corps of Engineers Cold Regions Research and Eng. Laboratory, and U. S. Army Natick Laboratories AND National Science Foundation			13. Type of Report & Period Covered 14.
15. Supplementary Notes			

16. Abstracts This report presents experimental results on the conditions of initiation of an ice jam by a simple surface obstruction, on the equilibrium thickness of an ice jam formed by accumulation and submergence of ice floes, and on the compression strength of floating, fragmented ice cover. In the study on ice jam initiation, it was found that the minimum concentration of floes in the opening of the obstruction at which a jam occurs is nearly independent of the ratio of width of constricted passage to channel width, and is proportional to a negative power of the ratio of floe length to width of constricted passage. From energy analysis of floe submergence, a relationship relating the thickness of a jam formed by accumulation and submergence of floes to the approach flow characteristics was derived and found to fit satisfactorily the experimental data. In experiments on compression strength of floating, fragmented ice cover it was found that the compressive strength is inversely proportional to compression velocity and independent of cover length.

17. Key Words and Document Analysis. 17a. Descriptors

Ice formation
Ice formation indicators
Floating Ice

17b. Identifiers/Open-Ended Terms

Ice jam initiation
Floe submergence
Ice cover compression strength

17c. COSATI Field/Group

18. Availability Statement	19. Security Class (This Report)	21. No. of Pages
No restriction on distribution. Available from National Technical Information Service, Springfield, VA 22161	UNCLASSIFIED	108
	20. Security Class (This Page) UNCLASSIFIED	22. Price 5.50

A LABORATORY INVESTIGATION OF THE MECHANICS AND HYDRAULICS OF RIVER ICE JAMS

by

J. C. Tatinclaux, C. L. Lee, T. P. Wang, T. Nakato,
and J. F. Kennedy

Sponsored by

U.S. Army Corps of Engineers Cold Regions Research and Engineering Laboratory, and U.S. Army Natick Laboratories
Contract No. DAAK03-75-C-0030

and

National Science Foundation
Grant No. ENG-72-04118A02

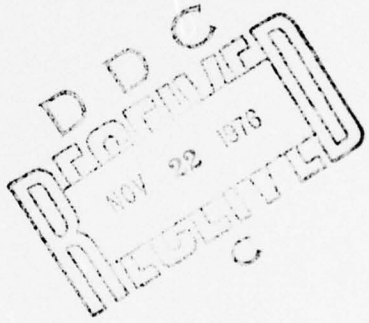

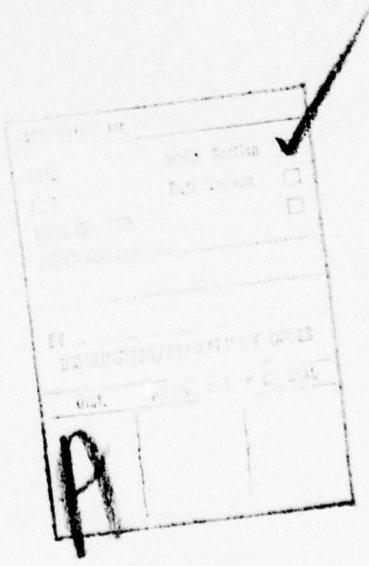

IIHR Report No. 186

Iowa Institute of Hydraulic Research
The University of Iowa
Iowa City, Iowa

March 1976

1a

ABSTRACT

This report presents experimental results on the conditions of initiation of an ice jam by a simple surface obstruction, on the equilibrium thickness of an ice jam formed by accumulation and submergence of ice floes, and on the compression strength of floating, fragmented ice cover.

In the study on ice jam initiation, it was found that the minimum concentration of floes in the opening of the obstruction at which a jam occurs is nearly independent of the ratio of width of constricted passage to channel width, and is proportional to a negative power of the ratio of floe length to width of constricted passage. The coefficient of proportionality and the negative exponent of this power function appear to depend upon the ratio of floe length to floe thickness, and to be strongly affected by the properties of the material of the laboratory floes, in particular by the interparticle friction or cohesive characteristics.

From energy analysis of floe submergence, a relationship relating the thickness of a jam formed by accumulation and submergence of floes to the approach flow characteristics was derived and found to fit satisfactorily the experimental data. The relationship predicts that a stable jam cannot be formed when the approach flow velocity exceeds a certain value. This phenomenon was observed experimentally, and the measured maximum values of approach velocity were found to be in excellent agreement with the predicted values.

In both studies on jam initiation and development, it was found that surface tension, and therefore the wetting properties of the material used for small laboratory floes, has a significant effect on the submergence velocity of small floes, and should be taken into consideration when small scale laboratory investigations of ice jam phenomena are to be conducted using floes made of artificial material.

Experiments on compression strength of floating, fragmented ice cover were conducted for ranges of cover length and cover thickness, using three different floe shapes and sizes. It was found that the

compressive strength is inversely proportional to compression velocity and independent of cover length. The effect of cover thickness and floe shape or size remains unclear partly because of the limited ranges of thickness and floe size investigated and partly because of the experimental scatter in the results.

ACKNOWLEDGEMENTS

The research reported herein was sponsored by the U.S. Corps of Engineers, Cold Regions Research and Engineering Laboratory, Hanover, N.H., through the U.S. Army Natick Laboratories, Natick, Mass., under Contract No. DAAK02-75-C-0030, and the National Science Foundation, under Grant No. ENG-72-04118 A02.

TABLE OF CONTENTS

LIST OF FIGURES

LIST OF SYMBOLS

Parts I and II

g	acceleration of gravity
h_e	depth of flow beneath an ice cover
h_n	depth of uniform flow in channel or flume
q_i	average surface discharge of ice = Q_i/t_i
t_e	average thickness of an ice cover
t_i	floe thickness
t_o	average submerged thickness of an ice cover
B	gap width in surface obstruction
C	aeral concentration of ice floes in flume = $Q_i h_n/\alpha Q_w t_i = q_i/V_s W$
C^*	critical aeral concentration
C_g	aeral concentration of floes in obstruction gap = $q_i/V_s B$
C_g^*	critical gap concentration of floes
F_r	Froude number = $V_n/\sqrt{gh_n}$
F_{cr}	critical Froude number for floe submergence = $V_c/\sqrt{gh_n}$
F_C	critical demsimetric Froude number for floe submergence (Eq. II-8)
F_D	densimetric Froude number (Eq. II-8)
L	larger plan dimension of ice floes
Q_i	volumetric discharge of ice
Q_w	water discharge in flume
V_c	critical submergence velocity of a floe
V_e	mean flow velocity beneath an ice cover
V_n	mean flow velocity in flume = Q_w/Wh_n
V_s	surface velocity in flume
W	flume width
α	ratio of surface velocity to mean flow velocity = V_s/V_n
β, γ	experimental coefficients
ρ	specific gravity of liquid water
ρ'	specific gravity of floes

Part III

d,b	lateral dimensions of an ice floe
d_e	effective diameter of an ice floe = $\frac{b}{d}\left(\frac{b+d}{2}\right)$
k_x	streamwise stress coefficient
t	thickness of fragmented ice cover
t_i	thickness of an ice floe
F	failure force of fragmented ice cover under compression
L	length of an ice cover
T_c	time of loading until failure of ice cover
V_c	velocity of the compression plate
W	width of ice cover
ε	strain = $\Delta L/L$
σ_{cr}	average compression strength of an ice cover
σ_x	longitudinal compressive stress
$\bar{\sigma}_z$	average vertical stress over jam thickness
ΔL	displacement of compression plate

A LABORATORY INVESTIGATION OF THE MECHANICS
AND HYDRAULICS OF RIVER ICE JAM

FOREWORD

An ice jam is an accumulation of ice on a stream which produces extensive blockage of the flow section. The accumulation is initiated by a channel obstruction which may consist of other ice, a change in channel alignment (channel constrictions, sharp bends...), or natural or man made obstacles in the stream (bridge piers, protruding abutments, levees, sand bars etc...). Pariset, Hausser, and Gagnon (1966) give the following description of the life of an ice jam:

> "As winter begins, large quantities of ice floes form on rivers flowing in cold regions. The floes are carried downstream by the current until they reach an artificial obstacle such as bridge pier in a low velocity zone, or a river section where slower surface currents and topography cause the floes to wedge, and result in the eventual build-up of a continuous ice bridge. As new floes arrive and come to rest on the ice bridge, the front of the cover proceeds upstream at a rate depending on the quantity of ice coming from upstream. . . In some sections where the velocity is slower, a relatively thin ice cover progresses quickly and smoothly, whereas in other sections considerably local thickening termed ice jamming always occurs before the progression of the cover can proceed upstream. . ."

Uzuner and Kennedy (1974) describe the evolution of an ice jam as follows:

> ". . . a jam is initiated when the downstream passage of floating ice being transported by a stream or a river is blocked by a bridge, change in channel alignment, shorefast ice, etc. Thereby an obstacle to passage of subsequent floes arriving at the section is produced and a jam is initiated . . . The floes arriving at the leading edge of this stationary cover may have sufficient momentum that they are submerged immediately . . . Alternately, the arriving ice blocks may come to rest at the leading edge of the cover. If the Froude number of the flow is sufficiently small, the floes will accumulate in a single layer. At large Froude numbers, however, the ice blocks will be submerged and transported beneath

> the cover . . . The blocks swept under the cover may come to rest near the upstream end of the cover to form a "hanging dam", . . . or be transported further downstream, either coming to rest at some location or possibly (but not usually) being swept clear under the jammed ice, past the channel obstruction, and continuing downstream . . . Now as the length of the jam is increased by the arrest of the newly arrived floes near its upstream end, the total streamwise external force applied to the jam upstream from any section will cause the jam to thicken by failure or "collapse" of the ice cover, until its shear and compressive strengths are great enough to balance the applied forces . . . During early stages of jam formation, while the depth is still relatively small and the velocity and Froude number of the approach flow are large so that arriving floes are being submerged, the ice cover may thicken by deposition of submerged blocks."

These descriptions suggest that the formation and evolution of a jam can be divided into three phases:

1) Jam initiation, when floating ice floes encounter an obstacle and form an ice bridge across the stream.
2) Jam growth, with increasing length and thickness, when arriving floes are arrested at the leading edge of the ice cover; these may underturn and be deposited on the underside of the cover if the flow velocity is large enough.
3) Jam collapse by internal failure, when the length and thickness of the ice cover due to accumulation (Phase 2) reach values for which the compressive and shear strengths of the cover are exceeded.

It is conceivable that Phases 2 and 3 of the jam evolution occur alternatively; that is, the accumulation of floes at the upstream end continues as long as the supply of ice to the jam is uninterrupted, and during this time the collapse described as Phase 3 occurs intermittently at different locations along the jam.

Uzuner and Kennedy (1974) derived expressions for the equilibrium thickness an ice jam attains for the case in which the thickness is governed by internal strength and the associated failure or collapse phenomenon. The present investigation is concerned mainly with the initiation stages of ice jams, which is treated in the first section of this report, and with the evolution of jams by accumulation and transport of floes beneath the

ice cover, which is reported in the second section of the report. The third section of the report presents results of experimental determination of the compressive strength of floating fragmented ice covers, a quantity which is of central importance in the prediction of the equilibrium thickness of a jam due to the internal failure the cover undergoes when the loading exceeds its strength.

I. INITIATION OF ICE JAMS BY PARTIAL SURFACE OBSTRUCTIONS

A. Introductory Remarks. The variety of channel obstructions which may cause arriving ice floes to form an ice bridge or arch across a stream channel is much too large for a single study to examine them all. The main goal of the present investigation was to gain an improved understanding of the initial phase of ice jam formation, and to determine the main parameters describing the flow conditions, obstruction configuration, and ice conditions which bear on the phenomenon of jam initiation. The obstruction chosen for the investigation consisted of a simple surface constriction in a uniform rectangular channel. A similar study has been reported by Calkins and Ashton (1974) of the Cold Regions Research and Engineering Laboratory (CRREL), who used plastic blocks as model floes.

In the present study experiments similar to those by Calkins and Ashton were conducted using real ice blocks as well as polyethylene blocks of identical shape and size. One of the purposes of the investigation was to determine whether the material used for the laboratory floes affects significantly the conditions under which a jam is initiated at a surface constriction in a uniform channel.

B. Experimental Apparatus and Procedure. The experiments on ice jam initiation were conducted either in the 40-foot long, 2-foot wide, 1-foot deep refrigerated flume located in the Low Temperature Flow Facility of the Iowa Institute of Hydraulic Research (IIHR) when natural ice blocks were used, or in a 30-foot long, 2-foot wide, 1-foot deep conventional, glass-walled flume when artificial ice blocks were used. Most of the experiments were conducted with parallelepipeds blocks of two different sizes. The plan dimensions were either 3 in. x 2.5 in. or 1.5 in. x 1.25 in. for both ice and plastic floes. The thickness of the floes was 3/8 in. for the plastic blocks and 5/16 in. for the ice blocks. The ice blocks were manufacturered in a commercial ice maker, and the plastic parallelepipeds were made from large, commercially available sheets of low density polyethylene. Additional tests were performed with paraffin parallelepipeds of dimension 1.75 in. x 1.75 in. x 0.5 in. The floes characteristics are summarized in the following table.

Table 1

Characteristics of the Experimental Floes

Material	Length L (in.)	Width b (in.)	Thickness t_i (in.)	Specific gravity ρ'
ice	1.5 3.0	1.25 2.50	0.313 0.313	0.92
low density polyethylene	1.5 3.0	1.25 2.50	0.375 0.375	0.91
paraffin	1.75	1.75	0.50	0.91

The device specifically designed and built to introduce the ice (real or artificial) blocks into the flumes consisted of a 5-foot long, 2-foot wide trough equipped with a piston which was fitted into the trough and was driven through a screw by a variable speed motor. Floes were loaded manually into the trough and uniformly distributed over the trough to insure that the ice discharge into the flow was nearly uniform once the piston was set in motion. Photographs of the ice-feeding apparatus in loaded condition is shown in figure 1. As the ice was pushed by the piston to the end of the trough, it fell onto an inclined screen, which was installed to avoid the splashing when free-falling floes hit the water surface, and entered the flow at a nearly steady rate. The discharge rate of ice could be adjusted by varying the piston speed and/or the depth of ice in the trough.

The surface obstruction was composed of two identical plywood boards attached perpendicularly to the walls of the flume near the downstream end of the flume test section. The gap in the obstruction was symmetric about the vertical longitudinal centerplane of the channel. Boards of different width were used to vary the width, B, of the gap between them. The boards were immersed by only 0.5 inch below the water surface, so that the mean flow velocity at the obstruction was nearly equal to that in the upstream, approach flow. A sketch of the experimental set-up is given in figure 2.

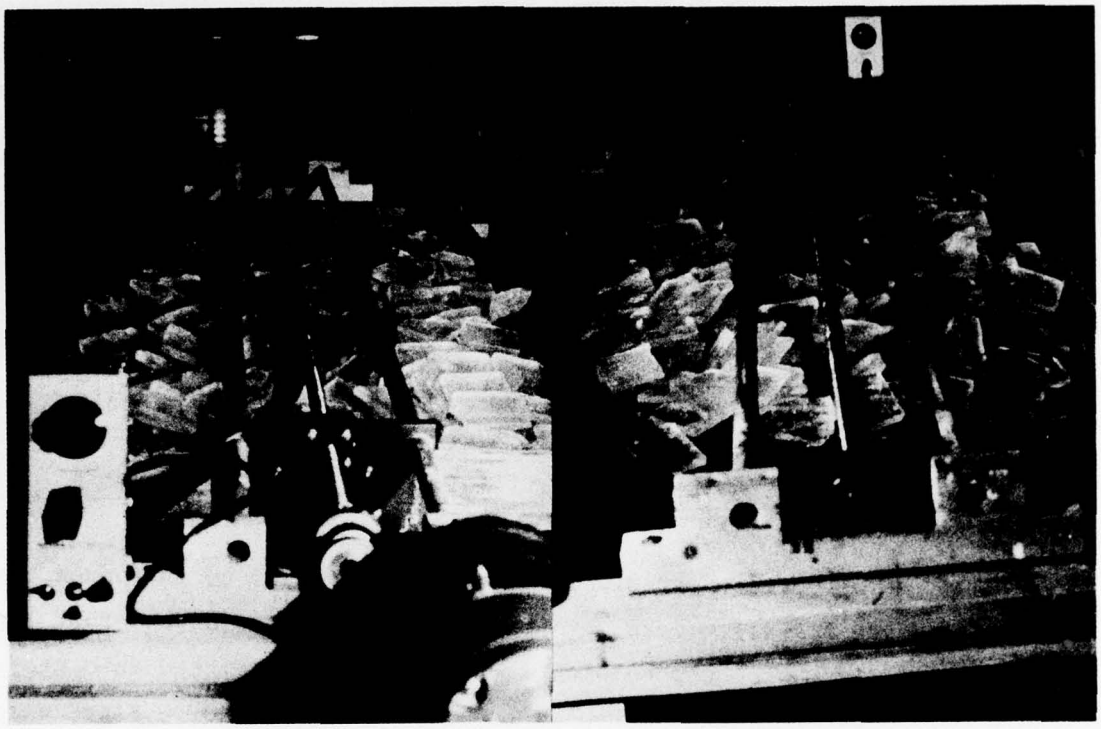

a) Ice Feeding Trough-Piston Apparatus

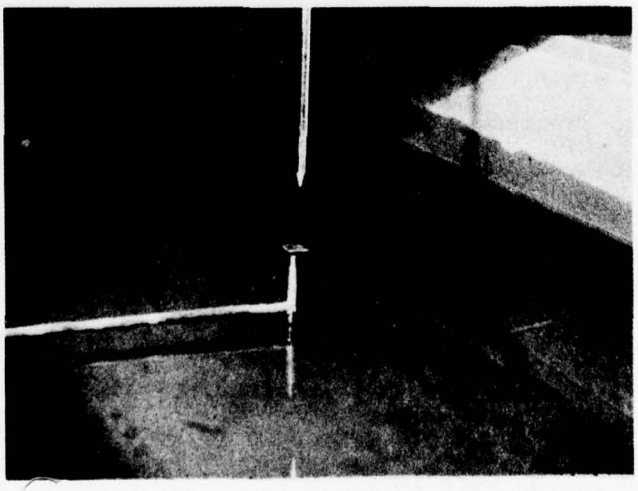

b) Jam Thickness Measuring Probe

Figure 1. Pictures of Experimental Apparatus for Ice Jam Studies

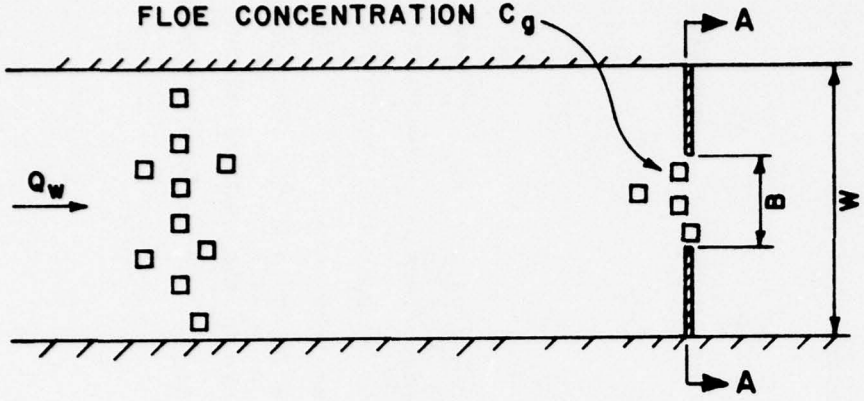

PLAN

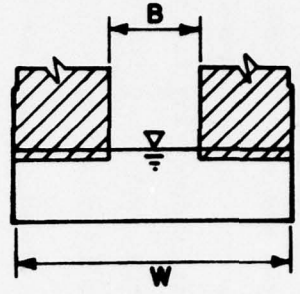

SECTION A-A

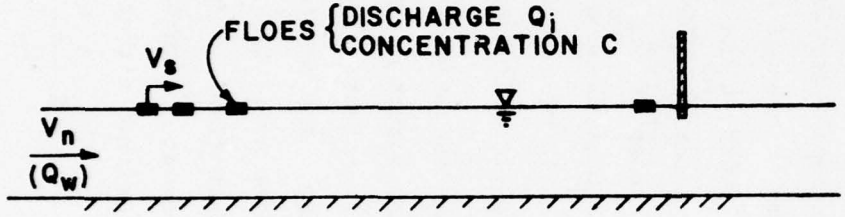

PROFILE

Figure 2. Definition Sketch for Ice Jam Initiation Study

In each run, ice floes were introduced into the flow at the desired areal concentration and a visual determination was made of the occurrence of arching at the obstruction. A jam was said to have been initiated when a stable arch formed across the gap in the channel obstruction and did not collapse under the impact of arriving floes. Several runs were performed for each set of experimental conditions to verify the reproducibility of the results. A typical jam is pictured in figure 3.

C. Dimensional Analysis. In the study of ice jam initiation, the independent variables to be taken into consideration are:

Q_w = water discharge in the flume, or V_n = mean velocity of flow or V_s = surface velocity
Q_i = volumetric discharge of ice
h_n = flow depth upstream from the obstruction
W = flume or channel width
B = gap width in the surface obstruction
L = characteristic length of the floes
t_i = thickness of the floes
g = acceleration of gravity
ρ = specific gravity of liquid water
ρ' = specific gravity of floes

Certain other properties of the material used to simulate the ice floes, such as the friction factor between floes, surface tension characteristics, etc., may also be important. The dependent variable is the occurrence of a persistent arch. The nondimensional parameters obtained from the independent variables are: L/B, t_i/h_n, B/W, h_n/W, $F_r = V_n\sqrt{gh_n}$ (Froude number of the approach flow), ρ'/ρ, and a measure of the surface concentration of the floes at the surface of the stream. The surface concentration of floes was defined either as

$$C = \frac{Q_i\, h_n}{\alpha Q_w\, t_i} = \frac{q_i}{V_s\, W}$$

in which $q_i = Q_i/t_i$ was the surface discharge of ice, and α was the ratio of surface velocity to mean velocity of the approach flow and was measured at 1.18 over a wide range of flow condition as shown in figure 4, or as

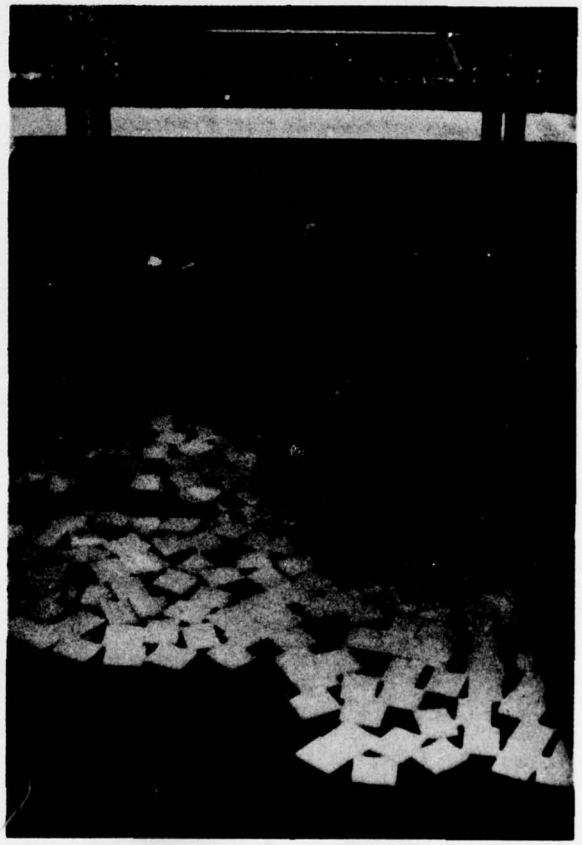

Figure 3. Typical Arching across Partial Surface Obstruction

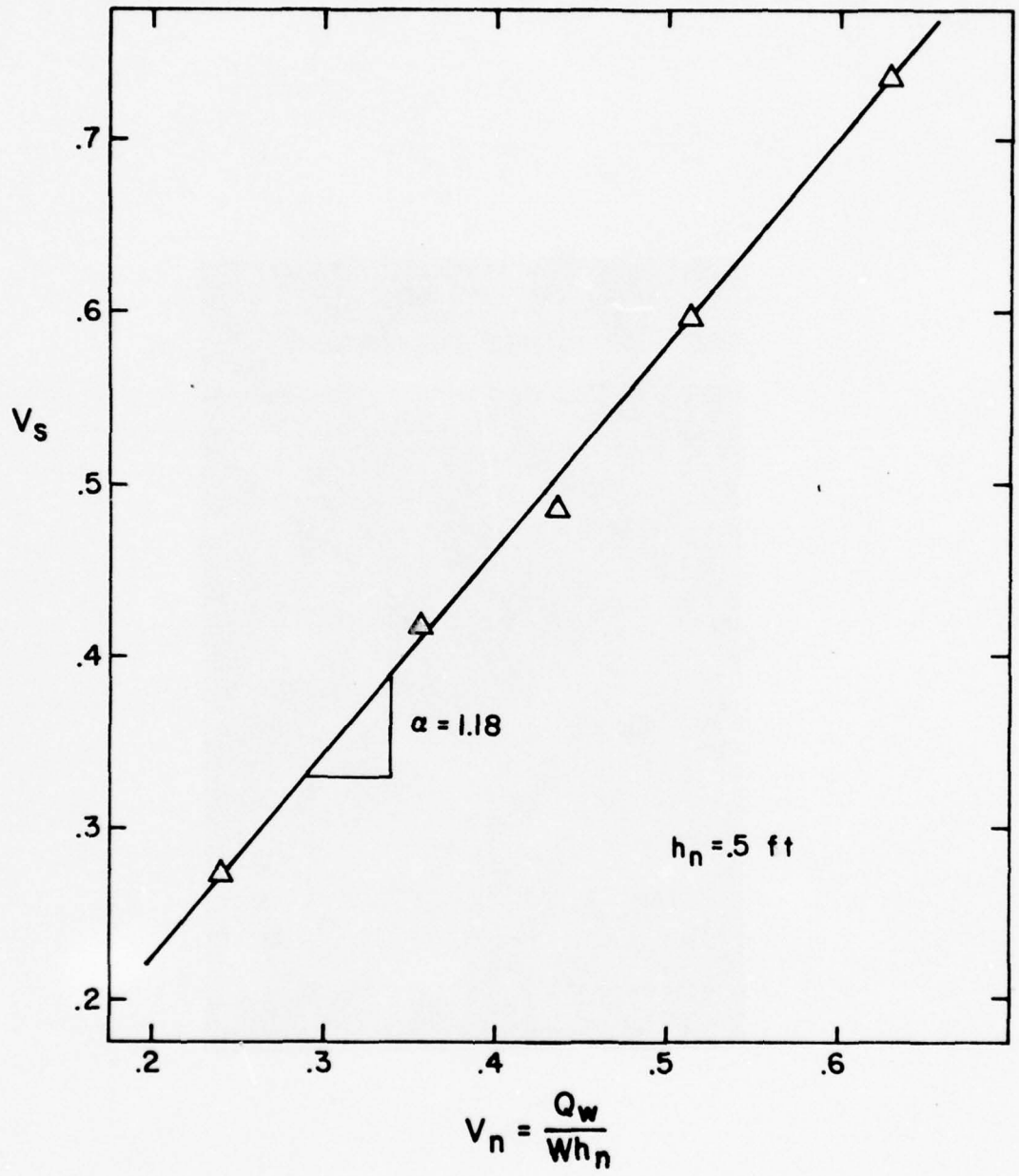

Figure 4. Surface Velocity versus Mean Flow Velocity in Experimental Flume

$$C_g = \frac{q_i}{V_s B} = C \frac{W}{B}$$

The parameter C is the average surface concentration of floes in the approach flow, while C_g is a measure of the areal concentration of floes in the obstruction gap. To these parameters should be added parameters describing the material properties of the floes.

In all experiments, the parameters t_i/h_n was kept constant, as was the quantity h_n/W. Since ice jam initiation is primarily a surface phenomenon it was judged that these two depth-related parameters have no significant influence on its occurrence. Therefore, the initiation of a ice jam by a surface obstruction of the type investigated here can be expressed by

$$J = J(C \text{ or } C_g, L/B, B/W, F_r, \text{material properties})$$

where J is a binary (yes or no) function. One can also define a critical floe concentration C* or C_g^* such that a jam will occur only when $C > C^*$ or $C_g > C_g^*$. This critical minimum floe concentration will be a function of the other parameters

$$C^* = F_1(L/B, B/W, F_r, \text{material properties})$$
$$C_g^* = F_2(L/B, B/W, F_r, \text{material properties}) = \frac{W}{B} F_1$$

D. Presentation of Results and Discussion. The experimental conditions are listed in Appendix A, which presents the values of the independent variables and of the dimensionless parameters. The last column of each table indicates whether a stable arch formed. As will be seen from the results and their graphical representation given in Figures 5 to 8, the results obtained with polyethylene parallelepipeds are quite different from those obtained with ice floes. This indicates that the material properties of the floes influence the formation of a jam. Indeed, the jams formed by the two different materials were observed to be initiated and to evolve in quite different manners.

1. Effect of B/W. Several experiments were performed to determine the influence of the relative width of the gap opening, reflected in the parameter B/W, on the minimum concentration above which

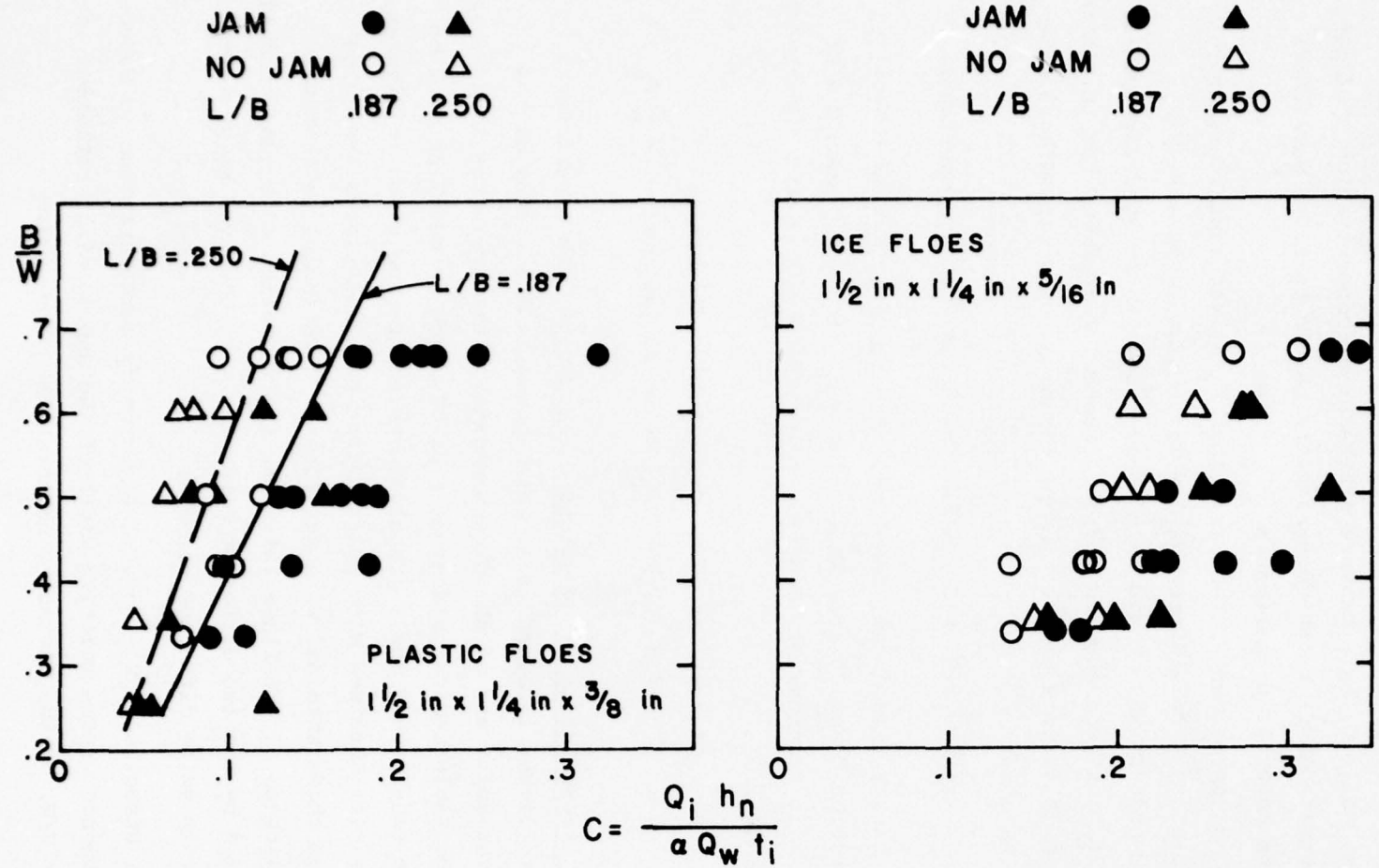

a) Plastic Floes

b) Ice Floes

Figure 5. Effect of B/W on Upstream Critical Areal Concentration C*

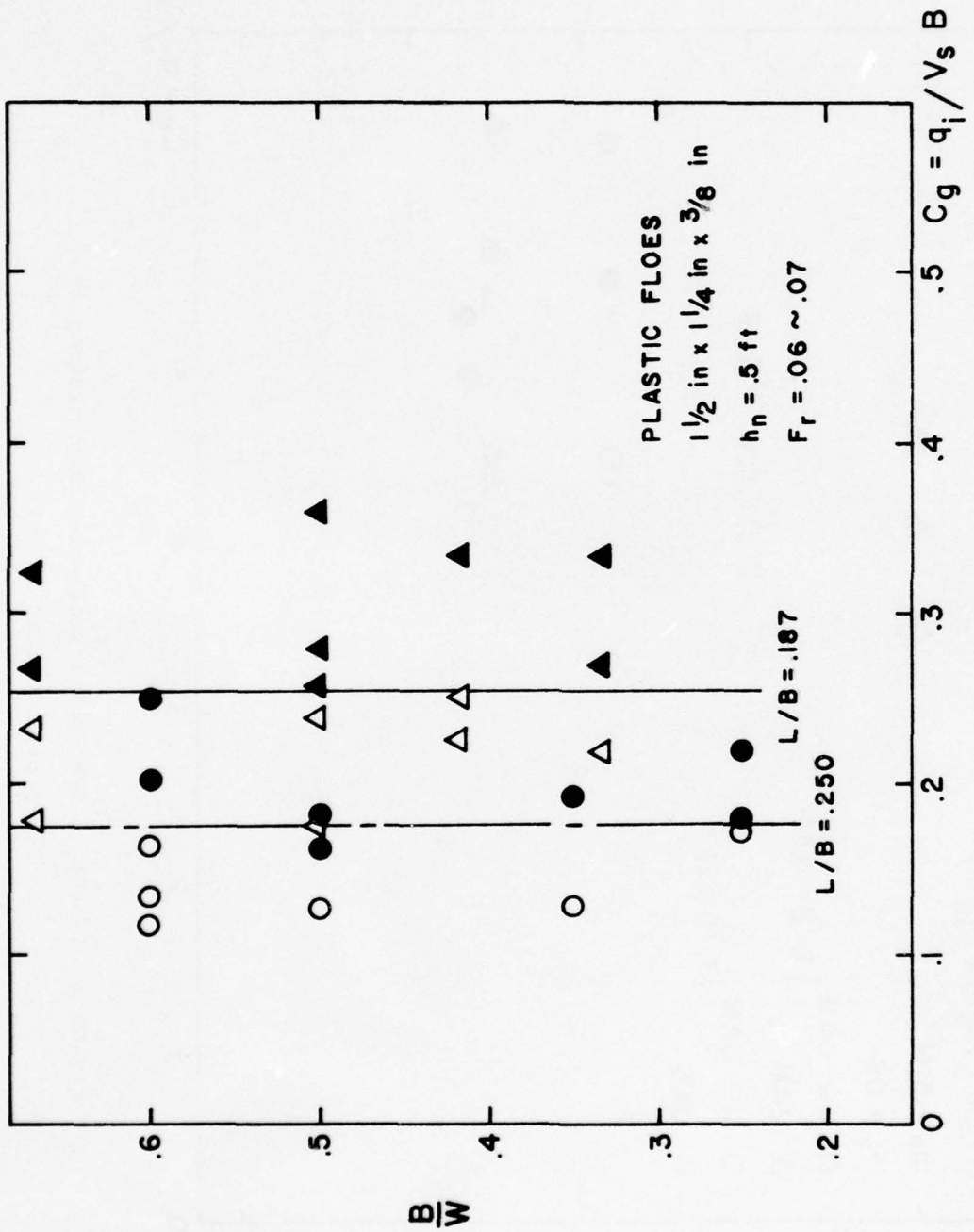

Figure 6. Effect of B/W on Critical Gate Concentration C_g^*

a) Plastic Floes

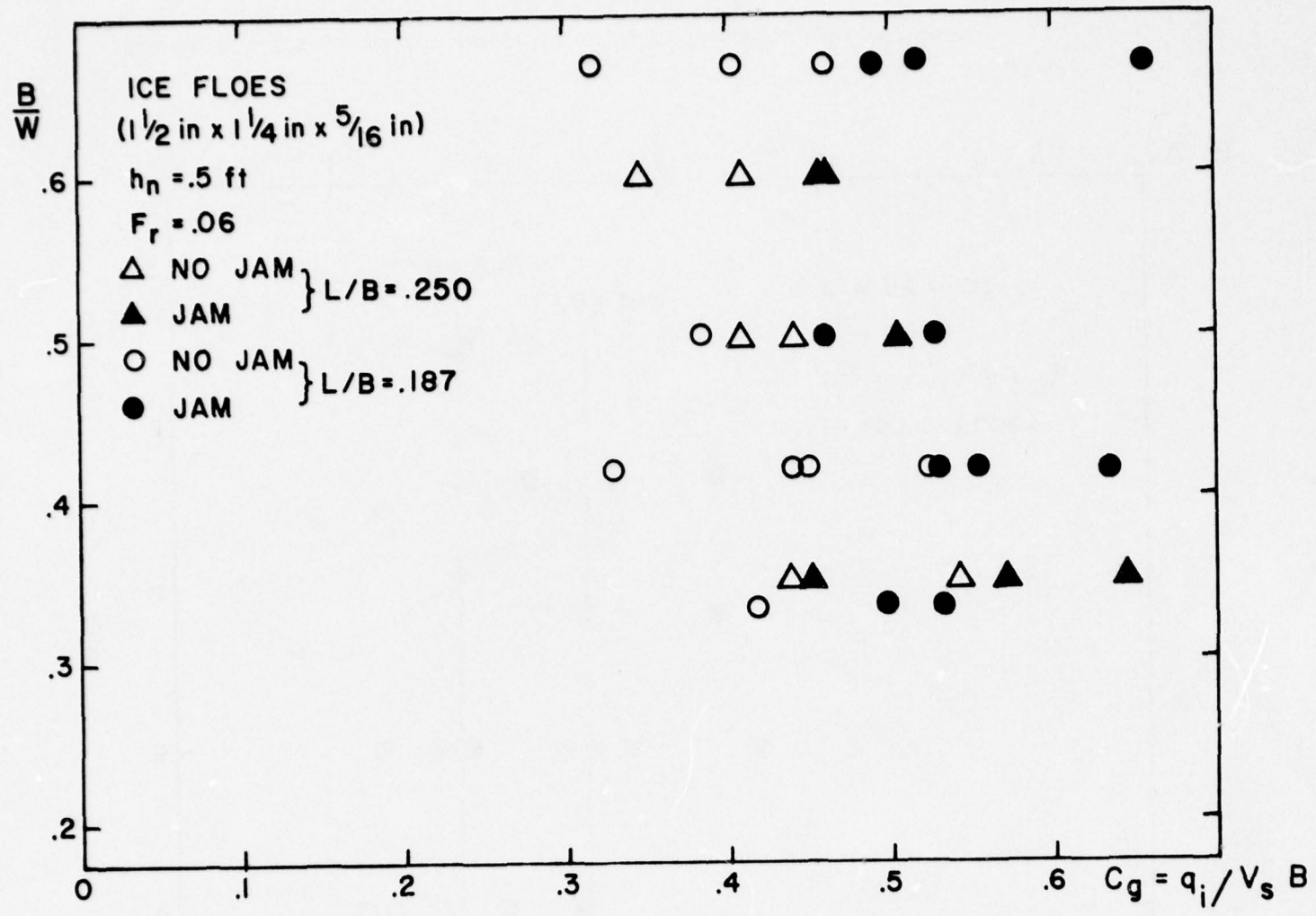

Figure 6. Effect of B/W on Critical Gate Concentration C_g^*

b) Ice Floes

arching occurs, C^* or C_g^*. In each series of these tests, the parameter L/B was kept constant. The floe size L was fixed, the gap width B was held constant, and the width of the flume was varied by installation of longitudinal partitions (internal walls) fabricated from aluminum plates. Experiments were run with the smaller floes at a Froude number $F_r = 0.06$ and two values of L/B: 0.250 and 0.187. The results of these tests are presented in figures 5a and 6a for plastic floes and in figures 5b and 6b for natural ice floes. Figures 5a and 5b give the critical concentration C^* versus B/W, while C_g^* is plotted versus B/W on figures 6a and 6b.

From the results obtained with plastic floes (figures 5a and 6a) it appears that the critical concentration C^* at which an ice jam will initiate is proportional to B/W and that the corresponding values of C_g^* ($C_g^* = C^* W/B$) is independent of B/W. The results obtained with natural ice floes (figures 5b and 6b) are not as definitive, the variation of C^* and C_g^* with B/W is more erratic, and only in an average sense can it be said that C^* varies linearly with B/W and that therefore C_g^* is independent of it.

These preliminary tests show that the parameter $C_g = q_i/V_s B$, which is a measure of the areal concentration in the opening in the obstruction, is a better indicator of the potential for jamming at the opening in a symmetrical obstruction than is the upstream areal concentration of the oncoming ice floes.

2. Effect of Froude number. The effect of the Froude number on jam initiation can be inferred from figures 7a and 7b for plastic floes and from figures 7c and 7d for ice floes. In these figures the critical values of $q_i/V_s B$ are plotted versus $F_r = V_n/\sqrt{gh_n}$. The critical Froude number for submergence of the floes used in the present study was measured to be 0.08 to 0.09 to ice blocks, and 0.11 to 0.12 for plastic floes. It can be seen in figures 7a and 7b that the floe concentration at the gate, C_g^*, at which arching occurs is independent of the Froude number for plastic floes as long as the Froude number is less than its critical value for submergence, as was assumed by Calkins and Ashton (1975) in a similar study. When the Froude number is larger than this critical value, the gate concentration at which a jam initiates is a rapidly

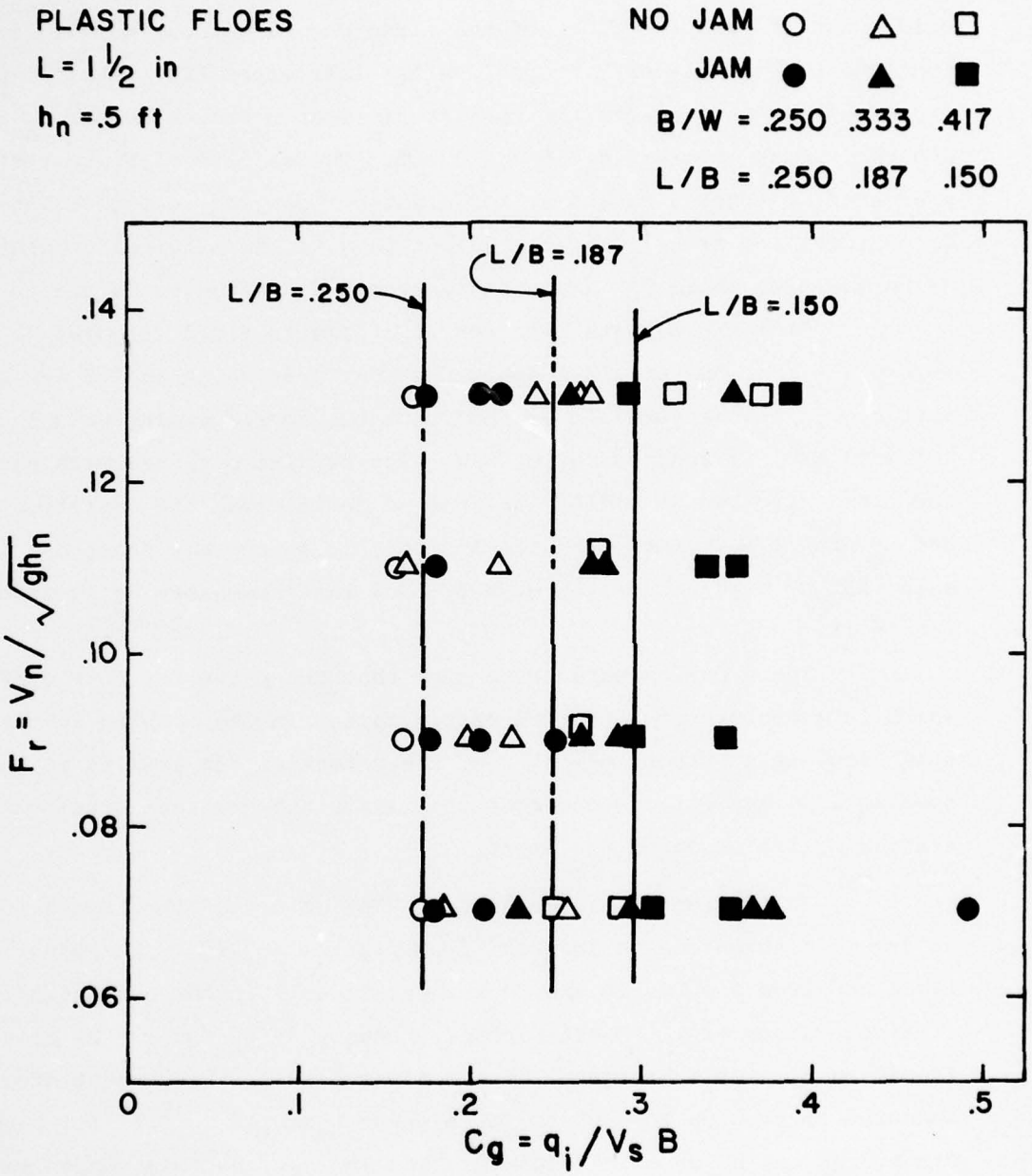

Figure 7. Effect of Froude Number on Critical Gate Concentration

a) Small Plastic Floes

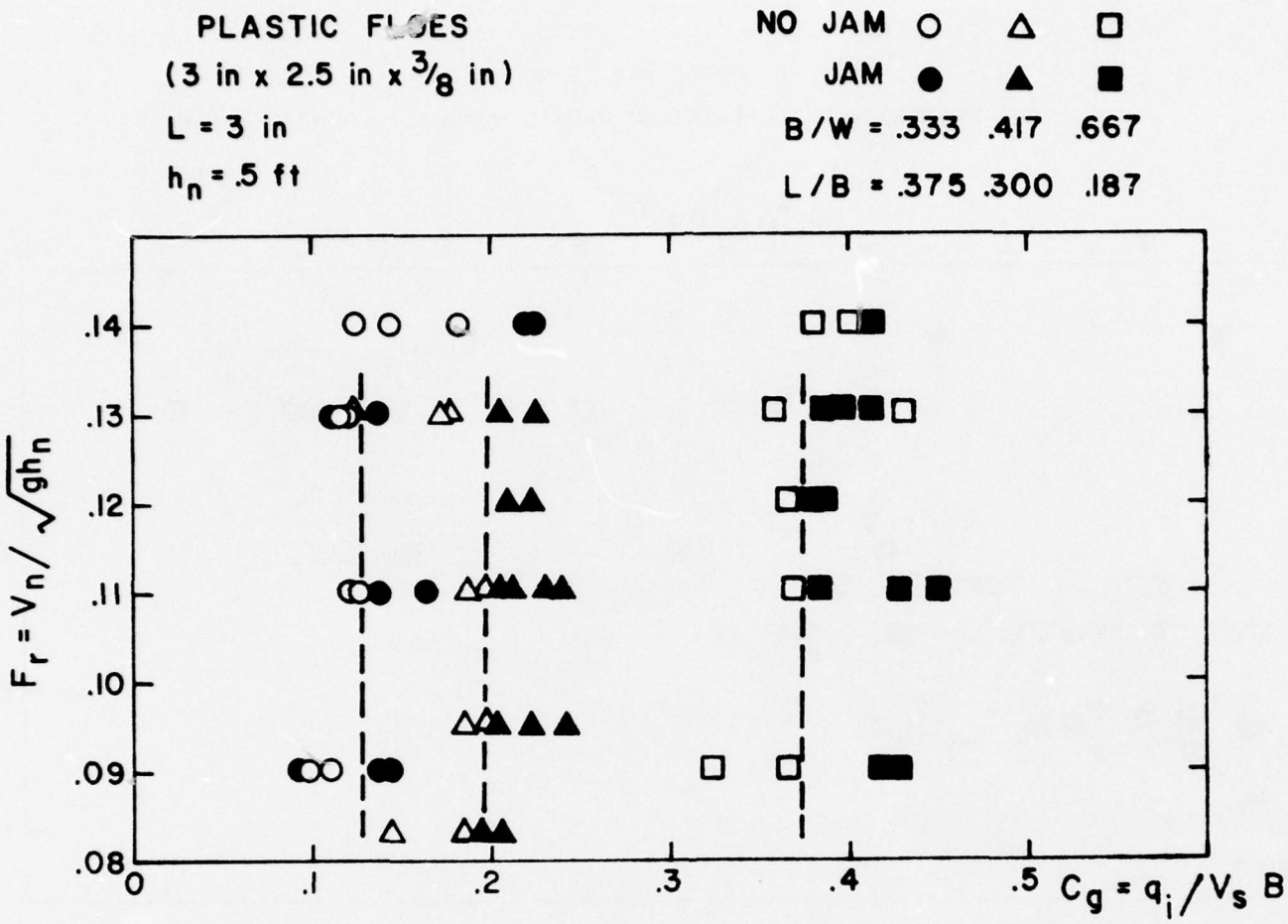

Figure 7. Effect of Froude Number on Critical Gate Concentration

b) Large Plastic Floes

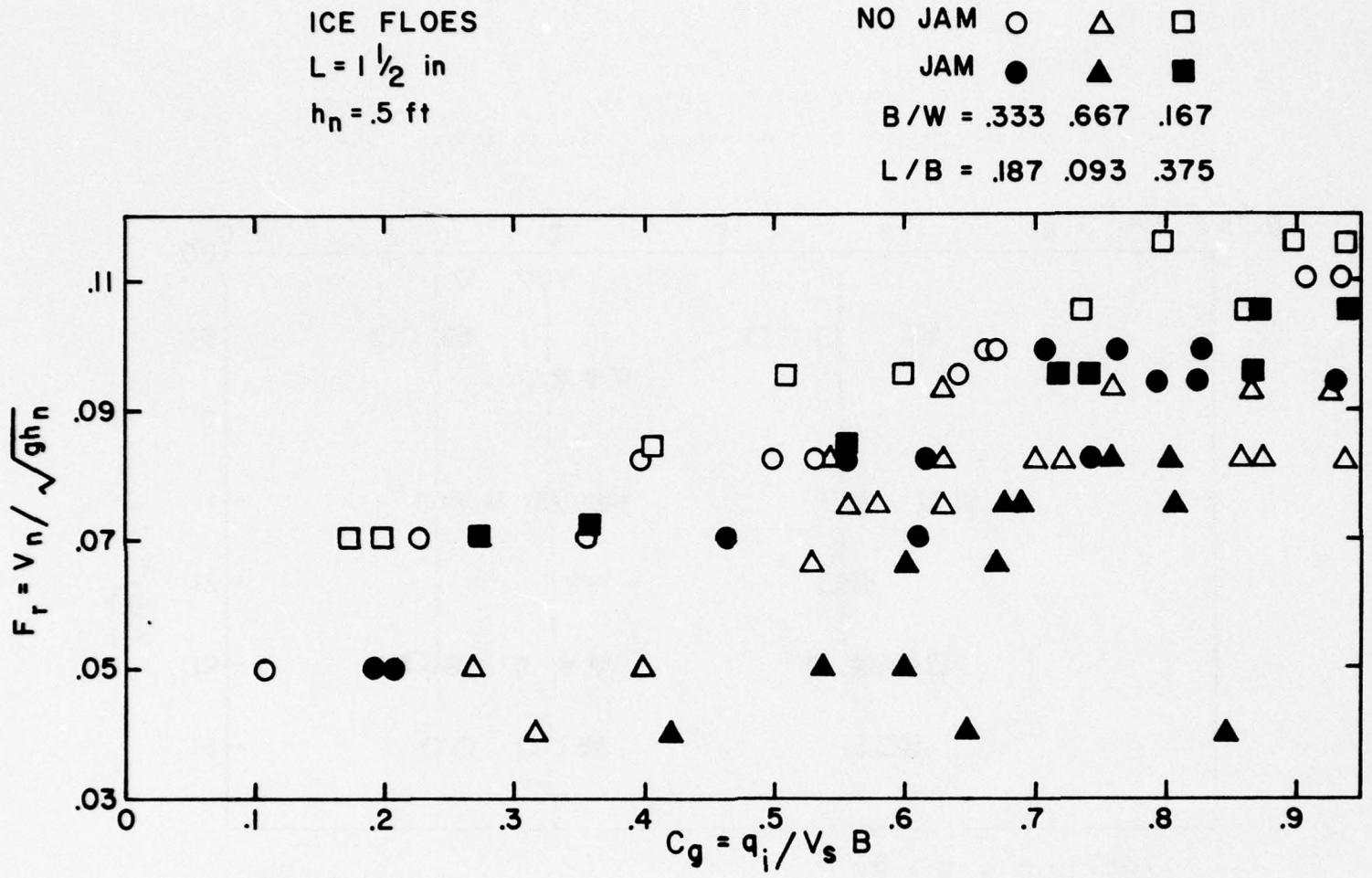

Figure 7. Effect of Froude Number on Critical Gate Concentration

c) Small Ice Floes

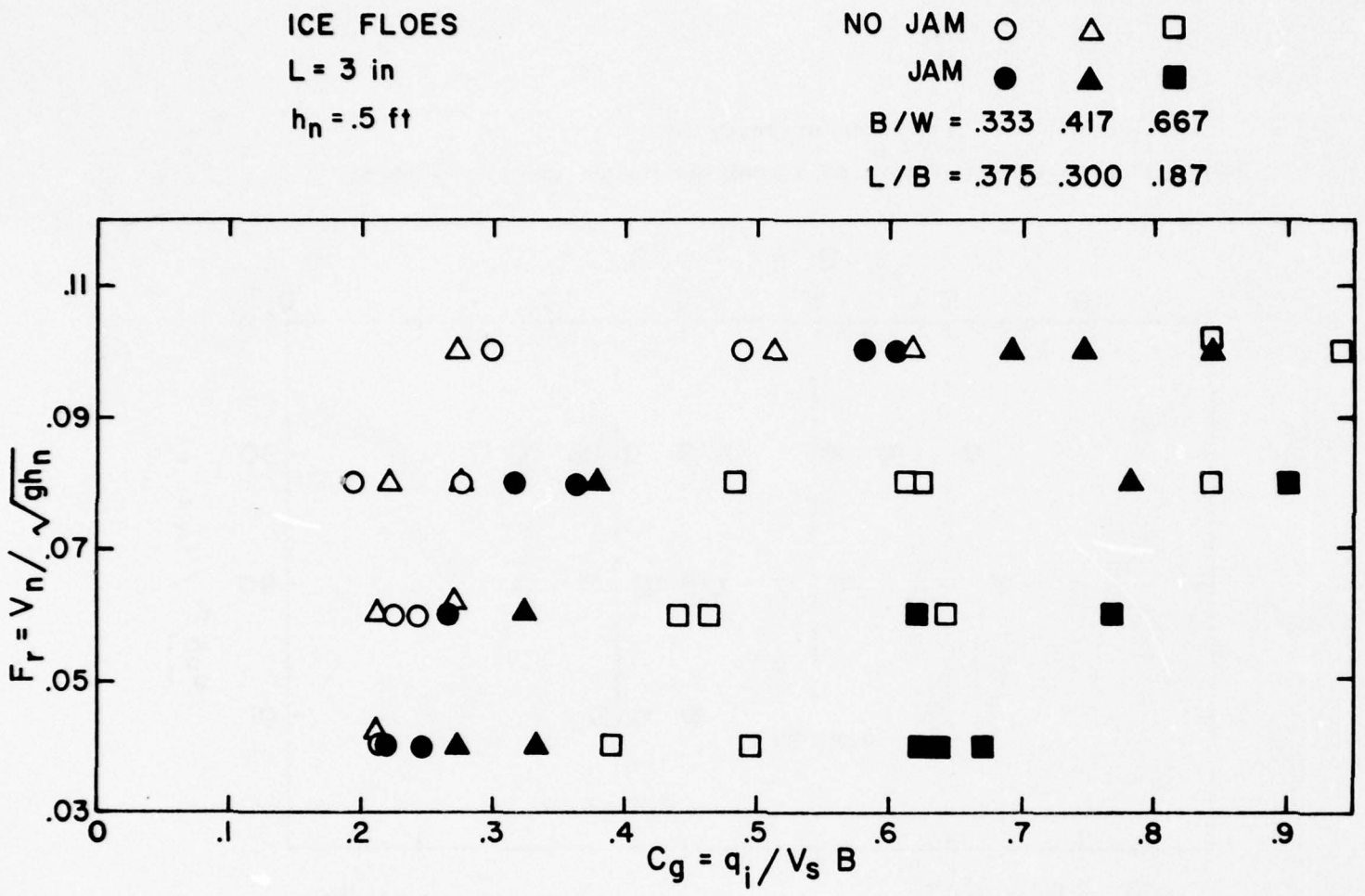

Figure 7. Effect of Froude Number on Critical Gate Concentration

d) Large Ice Floes

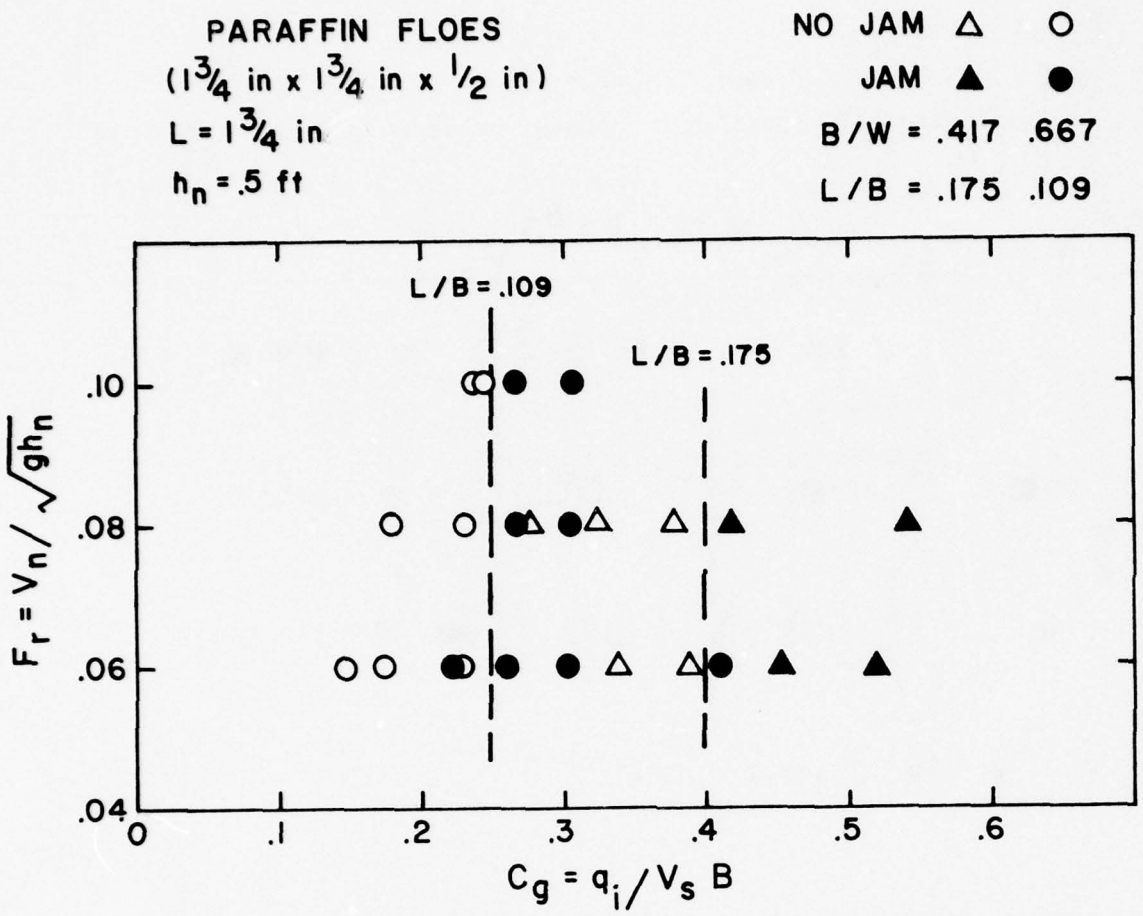

Figure 7. Effect of Froude Number on Critical Gate Concentration

e) Paraffin Floes

increasing function of the Froude number. In fact, with the amount of plastic floes available in the present experiments, no arching could be observed for the highest ice discharge possible at Froude numbers larger than 0.15, approximately, for upon impacting the surface obstruction the floes would be underturned and be swept underneath the gate.

The results obtained with real ice blocks (figures 7c and 7d) show variation of the critical gate concentration, C_g^*, with Froude number, even for values below the critical submergence Froude number of 0.08 to 0.09. This dependence is particuarly strong for the smaller ice floes, and for the larger values of B/W in the case of the bigger ice floes investigated. At lower values of B/W the results obtained with the larger ice floes indicate that C_g^* is also nearly independent of the Froude number for $F_r < 0.07$ approximately. It should also be noted that an estimate of C_g^* is even more difficult to determine with some confidence when ice blocks are used since over a rather wide range of values of $C_g = q_i/V_s B$, consecutive experiments performed under nominally identical conditions could lead to either arching or no arching. As a result an extremely large number of tests had to be performed to determine C_g^* for each set of test conditions when real ice floes were used.

The additional tests conducted with paraffin parallelepipeds and presented in figure 7e further confirm that, for artificial ice materials, the critical gate concentration C_g^* is independent of Froude number as long as F_r is less than its critical value for floe submergence.

3. Effect of L/B. The experimental data have been plotted as C_g versus L/B in figure 8a for plastic floes and in figure 8b for ice floes. In the latter figure only the results obtained for a value of the Froude number of 0.06 are presented. These log-log plots indicate that the critical gate concentration is a decreasing power function of the parameter L/B. Furthermore, the exponent of the function, given by the slope of the straight lines in the log-log plots, varies with the size of the floe; that is to say, for the same value of L/B the critical value C_g^* decreases with decreasing block size. No such variation of C_g^* with block size was reported by Calkins and Ashton (1975). Their equation to predict the critical C_g

$$\frac{q_i}{V_n B} = 0.01 \left(\frac{L}{B}\right)^{-2.56}$$

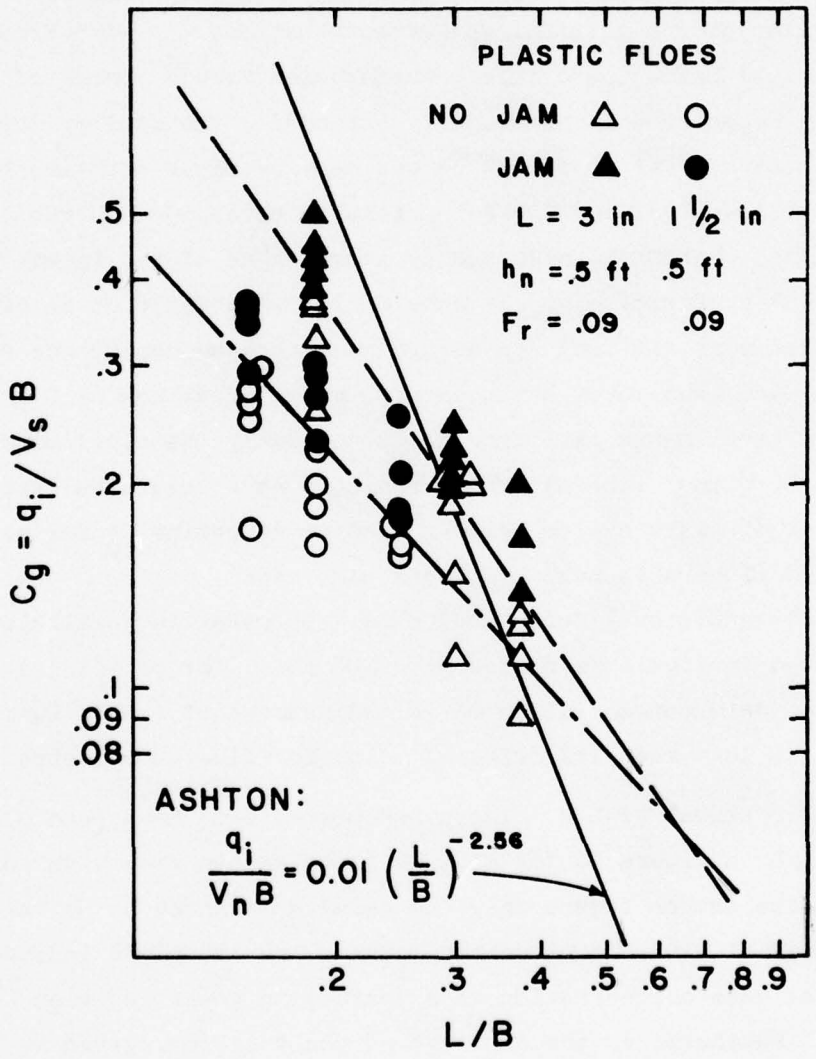

Figure 8. Effect of L/B on Critical Gate Concentration

a) Plastic Floes

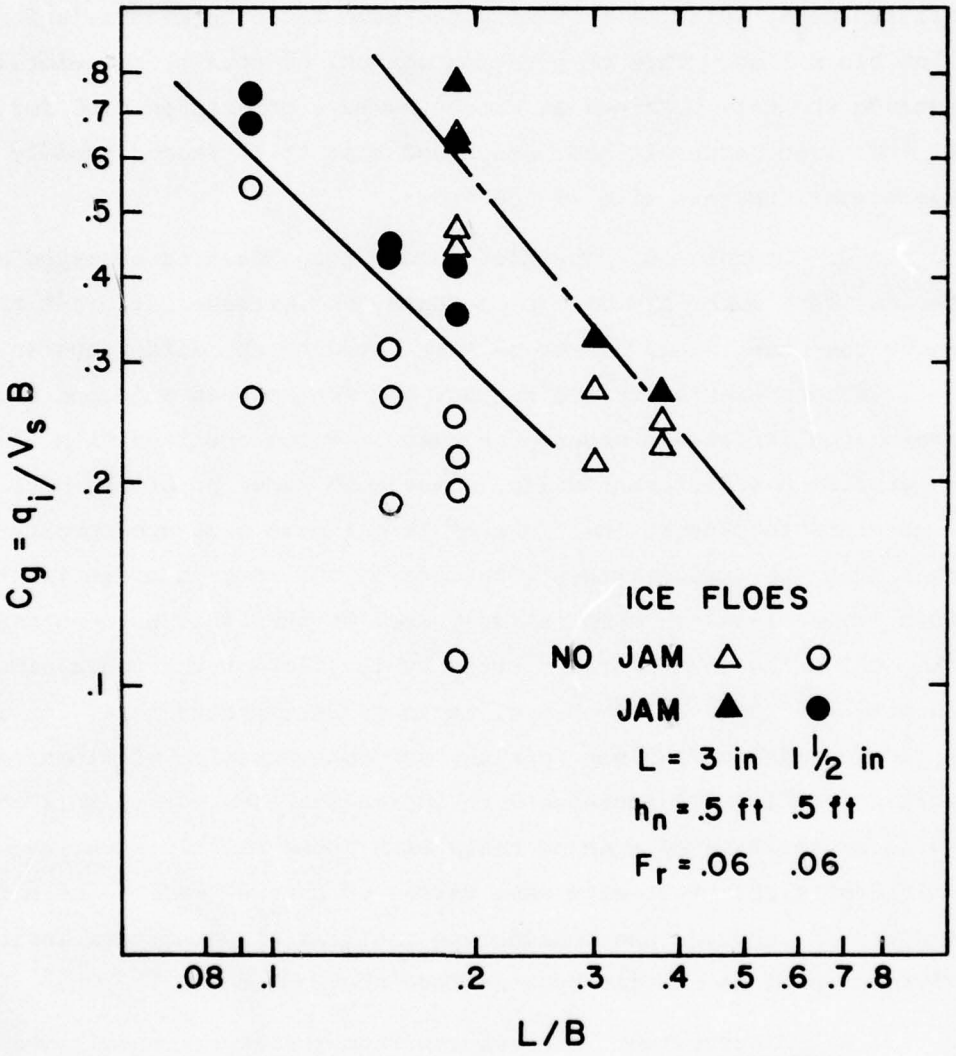

Figure 8. Effect of L/B on Critical Gate Concentration

b) Ice Floes

is plotted on figure 8a. It is seen that it does not conform well to the data obtained in the present experiments.

A comparison of figures 8a and 8b, shows that for floes of the same size but different material, the critical gate concentration obtained with the large block size is significantly higher for ice than for plastic parallelepipeds, while it is nearly the same for both materials for the smaller block size. This observation cannot, of course, be generalized to include the data obtained at Froude numbers other than 0.06 for the small ice floes, since it has been found that C_g^* increases rapidly with Froude number for this size of ice floes.

4. Discussion. The difference in the results observed between different block materials on the one hand, and between different block sizes on the other hand, has to be attributed to the difference in the friction forces exerted at the contact surface between adjacent blocks. Regarding the difference observed between results obtained with floes of same material but different sizes, since both types of blocks have the same absolute thickness, the floes of larger plan size are comparatively thinner than the smaller floes. Therefore, the interparticle friction force between larger floes is comparatively smaller than that between smaller blocks, while the shear force exerted by the flow on the under side of the blocks are comparable. Hence, it is to be expected that, for identical flow conditions and gap opening, the concentration of floes required to initiate a jam will increase with increasing floe size. This conjecture needs to be verified by running tests with geometrically identical blocks of different sizes; i.e. with same values of L/t_i as well as of L/B. The parameter L/t_i should then be added to the list of parameters influencing the formation of an ice jam by a surface obstruction.

E. Conclusions. The results from the experimental investigation of jam initiation by a surface constriction in a uniform, rectangular channel can be summarized as follows

1. The surface concentration of floes, C_g, in the opening in the obstruction is a better indicator of the potential for jamming than the upstream areal floe concentration, C,

since it is nearly independent of the relative flow constriction B/W.

2. The critical gate concentration C_g^* at which jamming occurs is a decreasing power function of the ratio L/B

$$C_g^* = a_o \left(\frac{L}{B}\right)^{-a_1}$$

The coefficient a_o and a_1 of the power function appear to be functions of L/t_i, ratio of floe length to floe thickness, and of the floe material. In particular a_1 appears to be an increasing function of L/t_i. More experiments are necessary to explicit the relationships between the coefficients a_o and a_1 and the parameter L/t_i.

3. Flow material properties are likely to affect the interparticle friction force and, as shown in Appendix C, can have a significant effect on the critical submergence velocity of floes. Therefore, small scale model studies of ice jamming conducted with artificial floes rather than real ice floes are likely to yield only qualitative results on the flow and ice discharge conditions conducive to ice jams.

II. THICKNESS OF ICE JAMS DUE TO ACCUMULATION AND TRANSPORT OF ICE FLOES

A. Introductory Remarks. After ice bridging occurs at a channel obstruction, an ice jam may be initiated and progress upstream as more ice floes accumulate at the leading edge of the ice cover. If the velocity of the arriving floes V_s is less than their critical velocity, V_c, the ice cover progresses as a single layer of floes; when V_s is larger than V_c, floes are submerged and deposited on the underside of the cover, as well as at its leading edge, producing fragmented ice cover several floes thick. The cover progresses by accumulation and deposition of ice floes until the resulting load at some section of the cover exceeds the strength of the cover. Internal collapse occurs and produces an increase in the ice jam thickness. This study of ice jam mechanics was concerned with determination

of the thickness that an ice jam may reach as a result of just submergence and deposition of the arriving floes.

The independent variables, which influence the development of an ice jam, and which are depicted in the definition sketch in figure 9, are the following:

h_n = approach flow depth

Q_w = water discharge or V_n = mean velocity of approach flow or V_s = surface velocity of approach flow

Q_i = volumetric ice discharge

ρ = specific gravity of liquid water

ρ' = specific gravity of floes

V_c = critical submergence velocity of floes

t_i = ice floe thickness

g = acceleration of gravity

The dependent variable is the average thickness of a jam along its uniform length, t_e. The flow depth, h_e, and velocity, V_e, beneath the ice cover can be expressed in terms of t_e, V_n and h_n as will be shown in section II-C.

B. Experimental Apparatus and Procedures. The experiments were conducted in the flumes described in Section I-B. Polyethylene and ice parallelepipeds of the same dimensions as those used in the jam-initiation study were used as ice floes, and were introduced into the flow using the ice feeding trough-and-piston mechanism described in Section I-B and shown in figure 1. In order to insure that an ice cover would form in the flume, a frame-mounted screen extending two-thirds of the flow depth below the water surface was installed at the downstream end of the test section of the experimental flume.

For specified upstream flow conditions, (i.e., given values of depth h_n and flow discharge Q_w), the volume of ice in the trough and the speed of the piston of the ice-feeding apparatus were adjusted to achieve a predetermined volumetric ice discharge, Q_i. The corresponding surface concentration of ice floes, C, in the approach flow is defined as in Section I-C by

$$C = \frac{Q_i \, h_n}{\alpha Q_w \, t_i} = \frac{q_i}{V_s \, W}$$

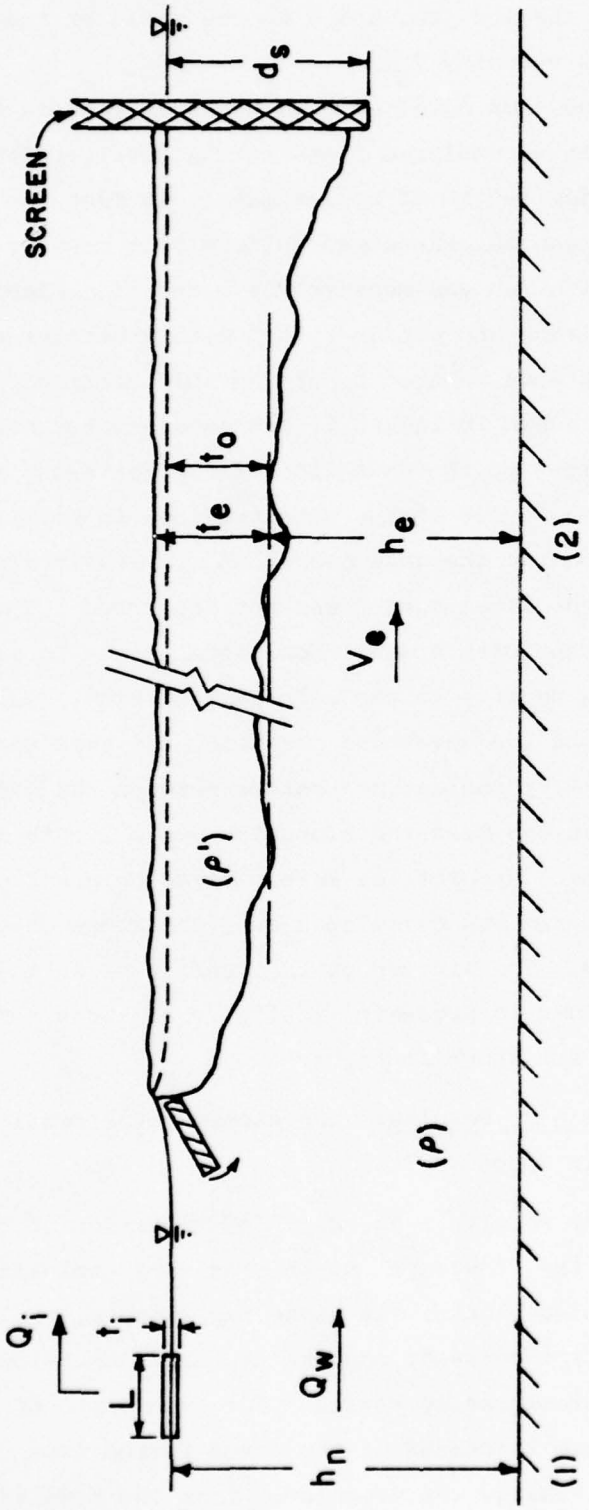

Figure 9. Definition Sketch for Ice-Jam Equilibrium Thickness Study

where $q_i = Q_i/t_i$ is the surface discharge of ice, W is the width of the flume, and therefore of the ice jam, and α is the ratio of the surface velocity V_s to mean flow velocity V_n.

Examples of ice jams obtained with plastic floes in the unrefrigerated flume and with natural ice floes in the refrigerated flume are shown in figure 10. A jam length of approximately 10 feet was considered adequate to insure that jam thickness was uniform over most of the length. The underside profile of a jam was measured by means of a specially designed hook gage attached to a rack-and-pinion fitted with a vernier gage. The rack-and-pinion supports were mounted on the movable carriage of the flumes. The hook gage, shown in figure 1, had an elongated horizontal arm which permitted measurement of the underside of the jam along the flume centerline while the support leg of the gage remained in proximity to one wall of the flume. By moving the gage slowly and carefully along the flume wall, the ice cover in the flume center was not disturbed. The sensing head of the gage was fitted with a small horizontal plate to provide more surface contact with the cover. In the refrigerated flume, where no visual observation beneath the cover was possible, the gage was raised until a resistance was felt, indicating contact between the gage and the ice cover. The jam thickness was measured along the whole length at intervals of approximately 1.0 inch. The profiles were plotted on graph paper and the average thickness of the jam was calculated over the range where the profile was more or less uniform. The picture of the profile of an ice jam obtained in the unrefrigerated flume is presented in figure 11; some representative measured cover profiles are shown in figure 12.

C. Presentation of Results. The experimental conditions and results are summarized in Appendix B.

1. Preliminary results. The depth of immersion of the screen was set at two-third of the flow depth on the basis of exploratory experiments conducted with wooden blocks. In these experiments, the flow depth and flow velocity were kept constant and the depth of immersion of the retaining screen was systematically varied. For each depth of immersion of the screen, the average thickness of the cover formed from a fixed average rate of block discharge was measured. From the results of these

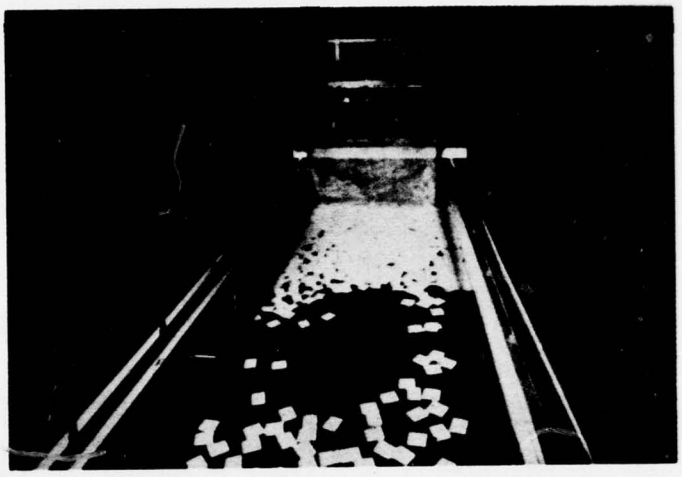

Figure 10. Pictures of Ice Jams in Experimental Flumes

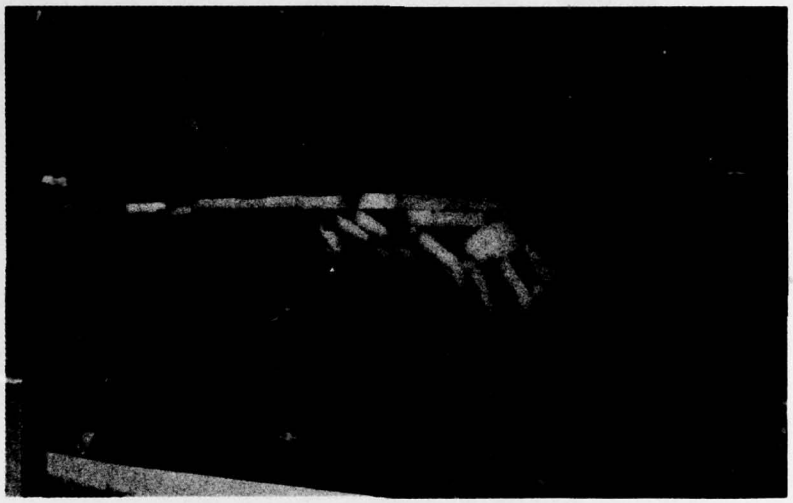

Figure 11. Picture of Jam Profile in Experimental Flume

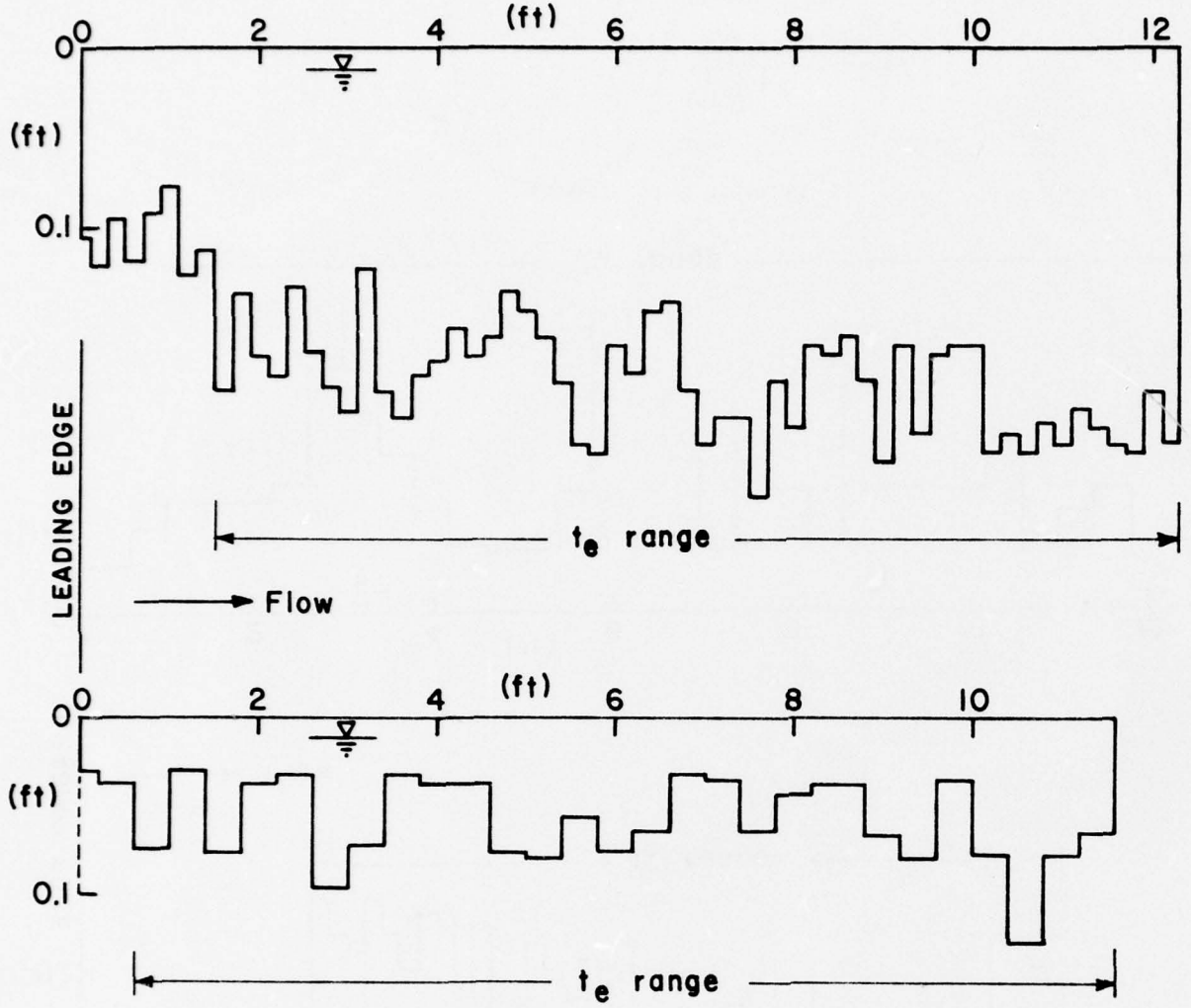

a) SMALL ICE FLOES

$h_n = 0.7$ ft

$F_r = 0.13$

$t_e = 0.204$ ft

$C = 0.72$

b) LARGE ICE FLOES

$h_n = 0.5$ ft

$F_r = 0.10$

$t_e = 0.065$ ft

$C = 0.58$

Figure 12. Typical Examples of Ice Cover Profiles

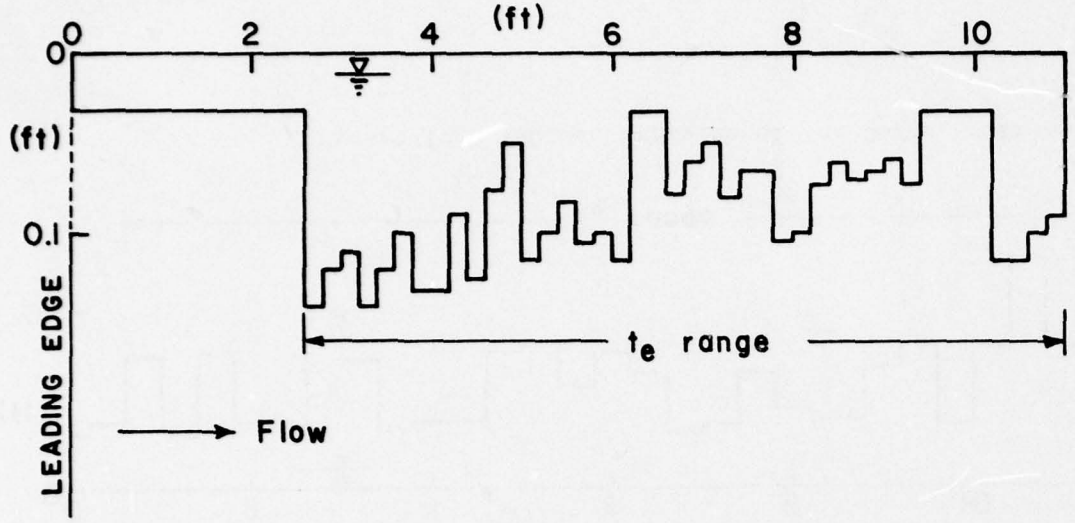

c) SMALL PLASTIC FLOES

h_n = 0.5 ft

F_r = 0.15

t_e = 0.094 ft

C = 0.13

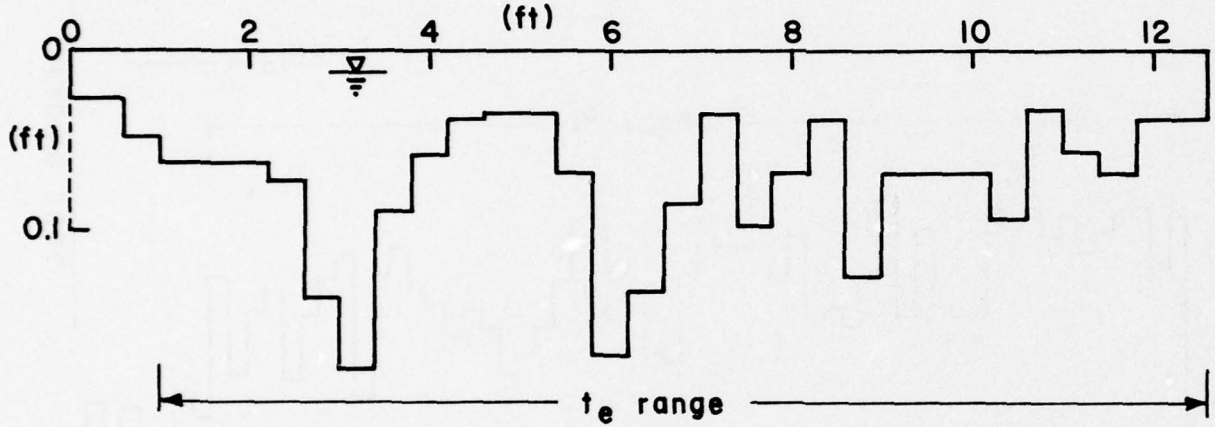

d) LARGE PLASTIC FLOES

h_n = 0.7 ft

F_r = 0.13

t_e = 0.083 ft

C = 0.62

Figure 12. continued

experiments, presented in figure 13, the ratio of screen depth to water depth was chosen to be 2/3, a value which was judged to be sufficient to initiate and retain a cover of any thickness attainable in the flume without inducing excessive local flow acceleration in addition to that due to the cover itself. The screen was important only in the initiation of ice jam formation; after the cover had progressed some distance upstream, the screen served only to prevent the jam from being swept along the flume channel.

2. Ice cover profiles. As might have been expected, the profiles, some representative examples of which are shown in figure 12, were found to be quite irregular. The individual floes came to rest on the underside of the cover generally in an inclined position rather than horizontally (see figure 11), and sometimes even formed hanging dams as profile "d" in figure 12 illustrates. In spite of these irregularities, the jam that formed were found to have fairly uniform thickness along their length, except near the downstream and upstream ends of the cover. At the screen some accumulation of floes took place, especially when the jam thickness was significantly smaller than the depth of screen immersion. During the early stage of jam formation, the local flow contraction produced by the screen caused the floes to submerge deeper. Some of these submerged floes were carried below the cover and trapped against the screen, resulting in increased cover thickness there. The nonuniform, transition section at the upstream end of a jam was in general quite short, with a typical length of two to four jam thicknesses. It was observed in the unrefrigerated flume, which is equipped with glass walls, that floes arriving at the leading edge of the jam are "impacted" against the jam, submerged, and come to rest rather abruptly beneath the arrested ice cover. It was found that it was virtually impossible to form a jam of length sufficient to yield a meaningful evaluation of its average equilibrium thickness, t_e, when the Froude number, $F_f = V_n/\sqrt{gh_n}$, was greater than about 0.13, when ice floes were used, and about 0.15 when plastic blocks were used: at first a few floes would accumulate against the screen, but the subsequent ones would submerge and be transported beneath this initial accumulation and then under the barrier. Submerging the screen to the full

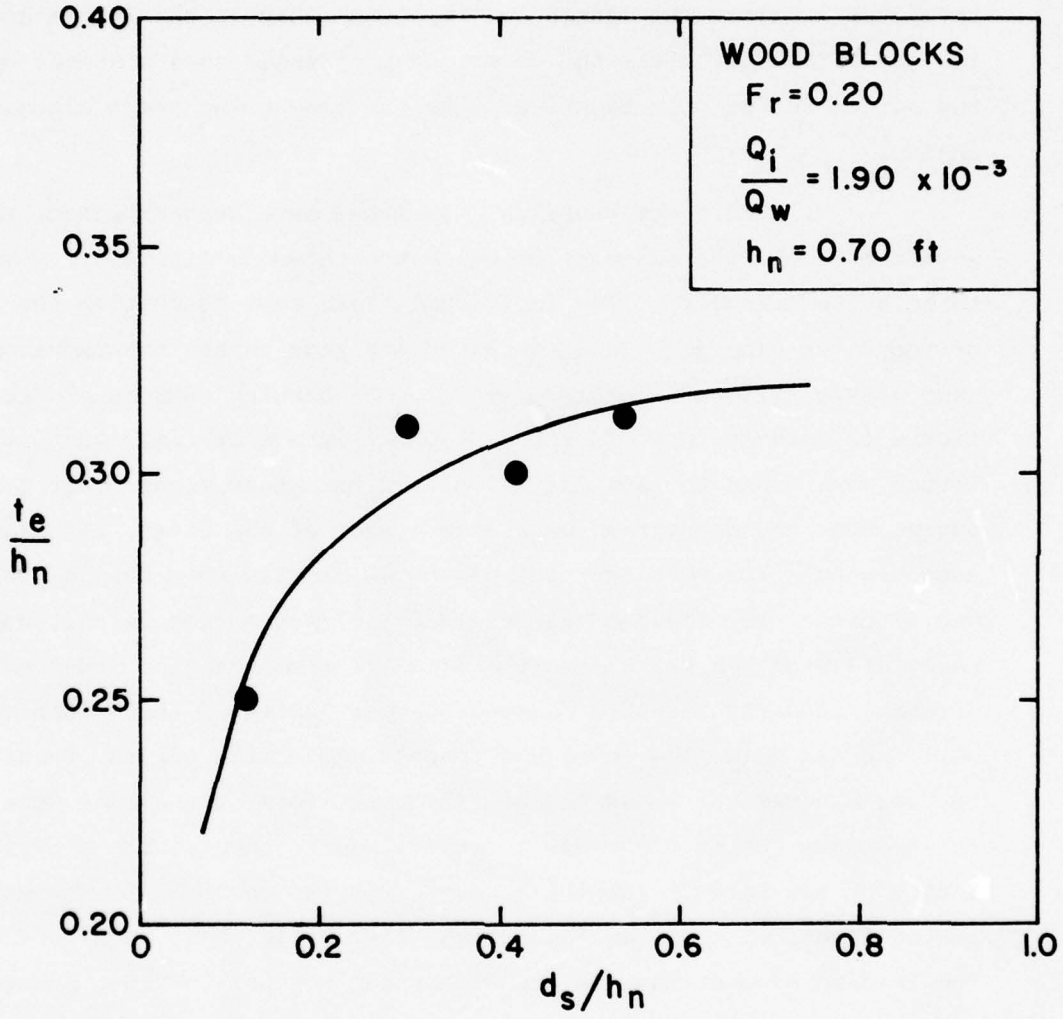

Figure 13. Effect of Screen Depth on Ice Jam Thickness (Wooden Blocks)

depth of the channel led to a complete obstruction of the channel by the blocks accumulating on the screen. The water level in the channel would rise and lift the accumulated ice until new equilibrium conditions were reached.

The results of the measurements of the average ice jam thickness t_e over the uniform reach of the jam are presented in figure 14a for ice floes and in figure 14b for plastic floes. The results are plotted as t_e/h_n versus surface concentration of the arriving floes, C, with the Froude number, F_r, as a parameter. From these figures it can be seen that over the range of concentration investigated, the jam thickness is practically independent of concentration. It should be mentioned that since the measurements of cover thickness are accurate only to within one floe-thickness, the corresponding error in t_e/h_n varies from $\pm$ 0.05 to $\pm$ 0.09, depending on the depth of flow. It can also be observed that the jam thickness generally increases with increasing Froude number; this effect of Froude number is more apparent in the data obtained with natural ice blocks. Finally the figures do not indicate significant variation of jam thickness with block size.

3. Energy analysis of floe submergence. An ice cover more than one floe thick can develop only if the floe velocity is larger than the critical velocity for submergence of a floe. When an arriving ice floe reaches the leading edge of an ice cover, part of its initial kinetic energy is dissipated in the impact with the arrested cover and part is transformed into potential energy as the floe submerges. However, as the floe submerges, it enters a zone of higher velocity due to the flow restriction produced by the ice cover. Therefore, the floe has some kinetic energy imparted to it by the surrounding flow. Hence it is reasonable to believe that the maximum depth of submergence of a floe and therefore the maximum potential energy it acquires should be directly related to the maximum kinetic energy which can be imparted to it by the flow. This can be expressed in equation form by

$$(\rho-\rho')\, g\forall\, (t_o-t_i) = \beta\rho'\forall\, \frac{V_e^2}{2} - \gamma \qquad \text{(II-1)}$$

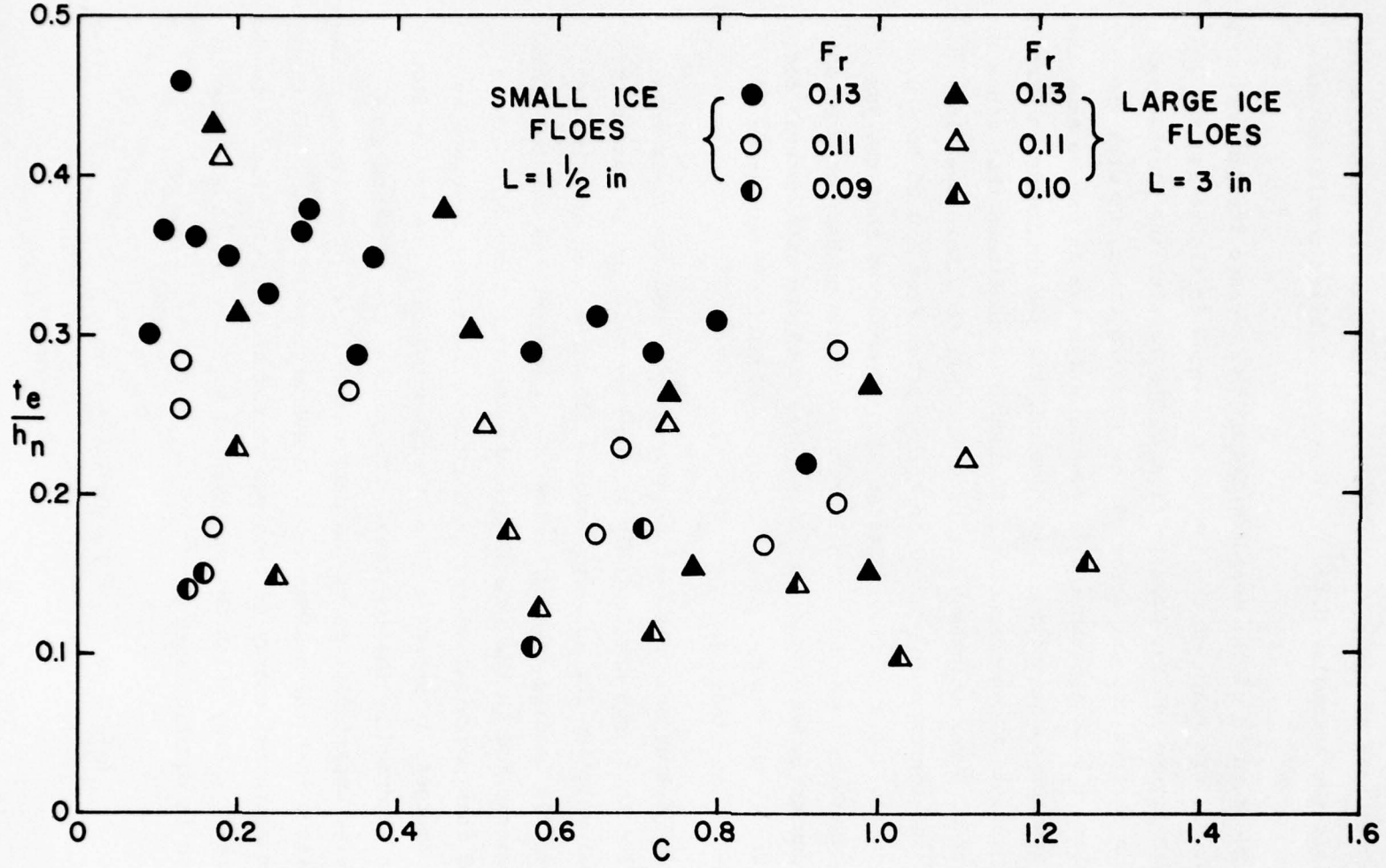

Figure 14. Variation of Jam Thickness with Upstream Areal Concentration

a) Ice Floes

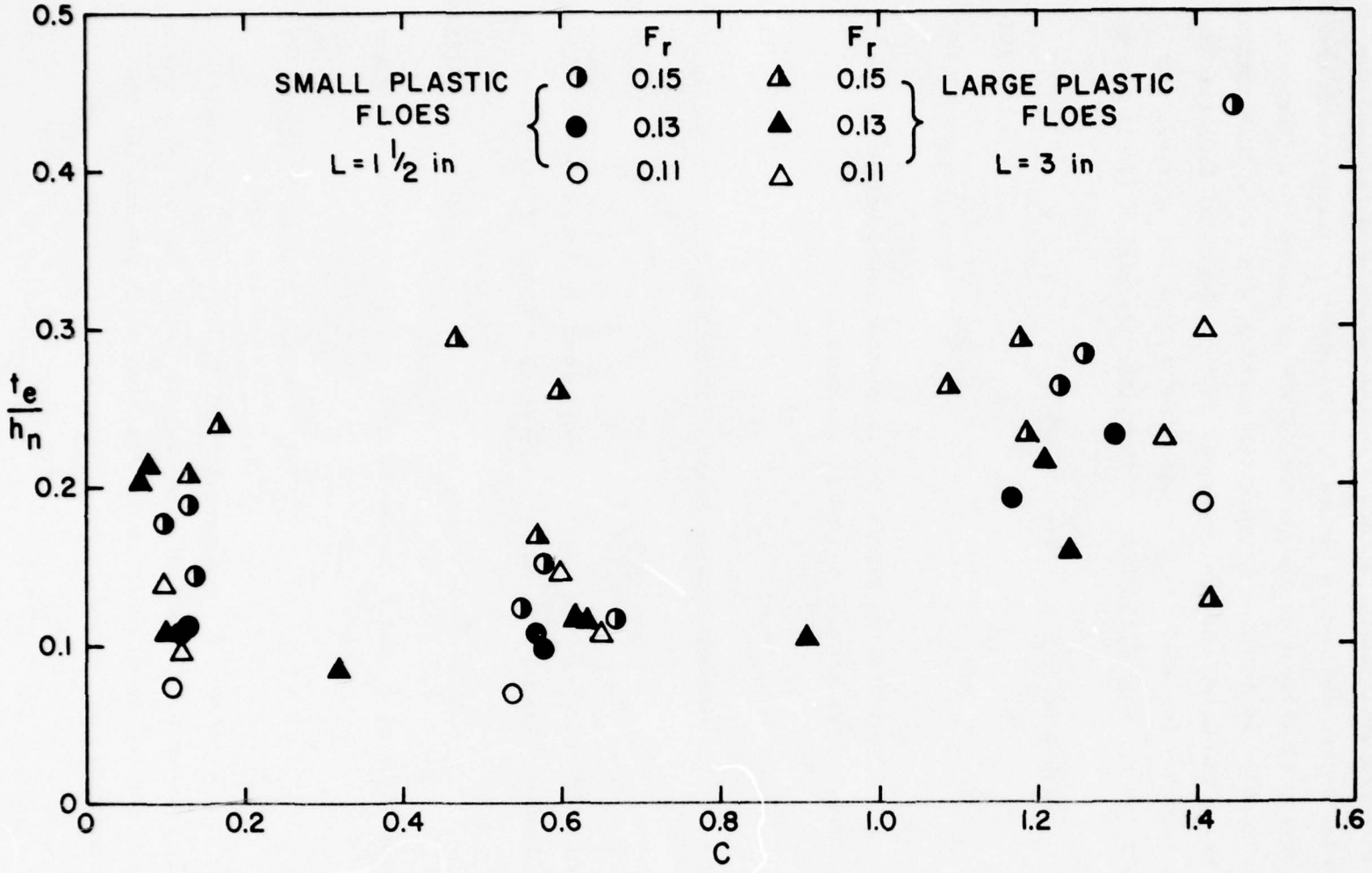

Figure 14. Variation of Jam Thickness with Upstream Areal Concentration

b) Plastic Floes

where β is a proportionality factor, $\forall$ is the volume of a floe and the other variables are defined in figure 9. The quantity γ represents the kinetic energy equivalent to the potential energy gained by a floe when its upper surface is level with the water surface, and "t_o", that thickness of floe below the water surface, is equal to "t_i" the total floe thickness. The flow velocity for which "t_o" is equal to "t_i" is the critical submergence velocity, V_c, of the floes. Thus, the expression (II-1) becomes

$$(\rho-\rho')\, g\forall(t_o-t_i) = \beta\rho'\forall\left(\frac{V_e^2}{2} - \frac{V_c^2}{2}\right) \qquad V_n > V_c$$

$$\frac{\rho'}{\rho}\, t_i \leq t_o \leq t_i \qquad V_n < V_c \tag{II-2}$$

If the pressure distribution within the fragmented ice cover below the water surface is hydrostatic, t_o and t_e are related by

$$\rho t_o = \rho' t_e \tag{II-3}$$

Continuity of flow between section 1 and section 2 in figure 9 yields

$$h_n V_n = h_e V_e \tag{II-4}$$

Furthermore, if energy losses over the short reach of nonuniform thickness near the leading edge of the jam are neglected, the energy equation gives

$$h_n + \frac{V_n^2}{2g} = t_o + h_e + \frac{V_e^2}{2g} \tag{II-5}$$

After elimination of t_o and V_n between (II-3) and (II-4), (II-5) becomes

$$\left(\frac{h_e}{h_n}\right)^3 + \left(\frac{\rho'}{\rho}\frac{t_e}{h_n} - 1 - \frac{V_n^2}{2gh_n}\right)\left(\frac{h_e}{h_n}\right)^2 + \frac{V_n^2}{2gh_n} = 0 \tag{II-6}$$

Since the Froude number of the approach flow, $F_r = V_n/\sqrt{gh_n}$, is small, (typically between 0.08 and 0.15), the terms $V_n^2/2gh_n$ may be neglected in (II-6), and the following equation for the flow depth beneath the ice cover is reached:

$$\frac{h_e}{h_n} = 1 - \frac{\rho'}{\rho}\frac{t_e}{h_n} \tag{II-7}$$

Introducing this expression into (II-1) yields

$$\frac{\rho'}{\rho}\frac{t_e}{t_i} - 1 = \beta\left[\frac{V_n^2}{2g\frac{\Delta\rho}{\rho'}t_i\left(1 - \frac{\rho'}{\rho}\frac{t_e}{h_n}\right)^2} - \frac{V_c^2}{2g\frac{\Delta\rho}{\rho'}t_i}\right] \qquad \text{(II-8)}$$

or

$$T = \beta\left[F_D - F_C\right]$$

The critical velocity of submergence for the floes was found to vary from 0.30 to 0.36 ft/sec, approximately, for ice floes and from 0.44 to 0.48 ft/sec, approximately, for the plastic blocks. Because V_c could not be determined with a high degree of precision, the experimental data first were plotted as T versus F_D as shown in figure 15. In the plot, two straight lines were fitted by the least-squares method through the data obtained with real ice blocks and with polyethylene parallelepipeds, respectively. The equation of the straight lines are

$$T = 1.62\ F_D - 0.96$$

with a correlation coefficient of 0.92, for ice floes, and

$$T = 1.44\ F_D - 1.76$$

with a correlation coefficient of 0.89, for the plastic blocks.

From the intercepts of the straight lines with the horizontal axis, an estimate of the critical submergence velocity for the ice floes and plastic blocks can be obtained by setting in $F_D \frac{\rho'}{\rho} t_e$ equal to t_i and neglecting the term $\frac{\rho'}{\rho}\frac{t_i}{h_n}$, which is usually very small compared to unity. The results are $V_c = 0.28$ fps for ice blocks and $V_c = 0.48$ fps for plastic blocks. These are in excellent agreement with the values measured experimentally.

Using the values of F_C of 0.58 and 1.22 for ice and plastic blocks, respectively, determined from figure 15, the data were replotted on figure 16 as T versus $(F_D - F_C)$. The slope β of the straight line which gives the best fit by the least-squares method with all data was computed to be equal to 1.59, and the correlation coefficient to be 0.93.

The scatter present in figures 15 and 16 is appreciable. It should be realized that the jam thickness is measured with a resolution

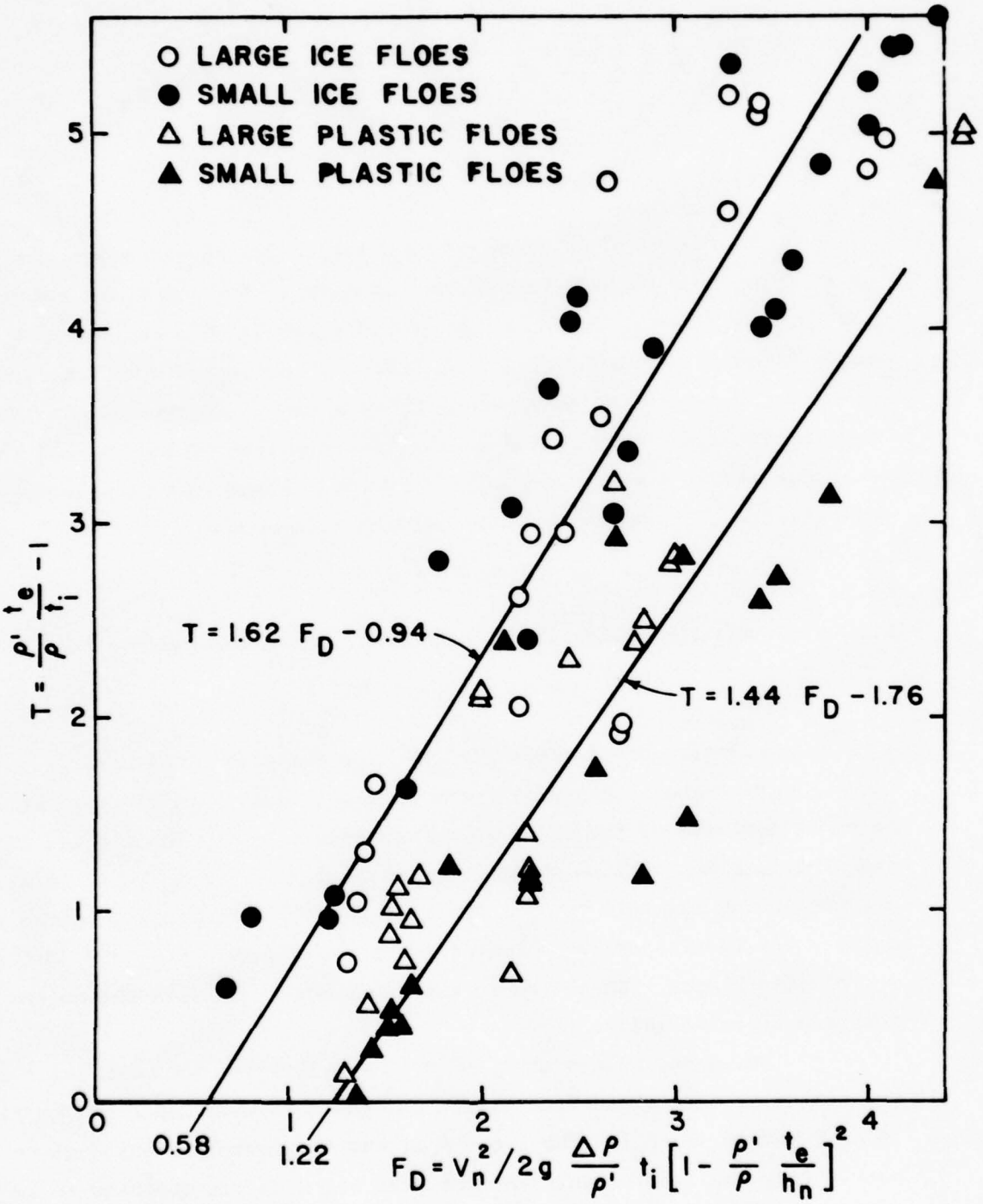

Figure 15. Dimensionless Ice Jam Thickness T as a Function of F_D

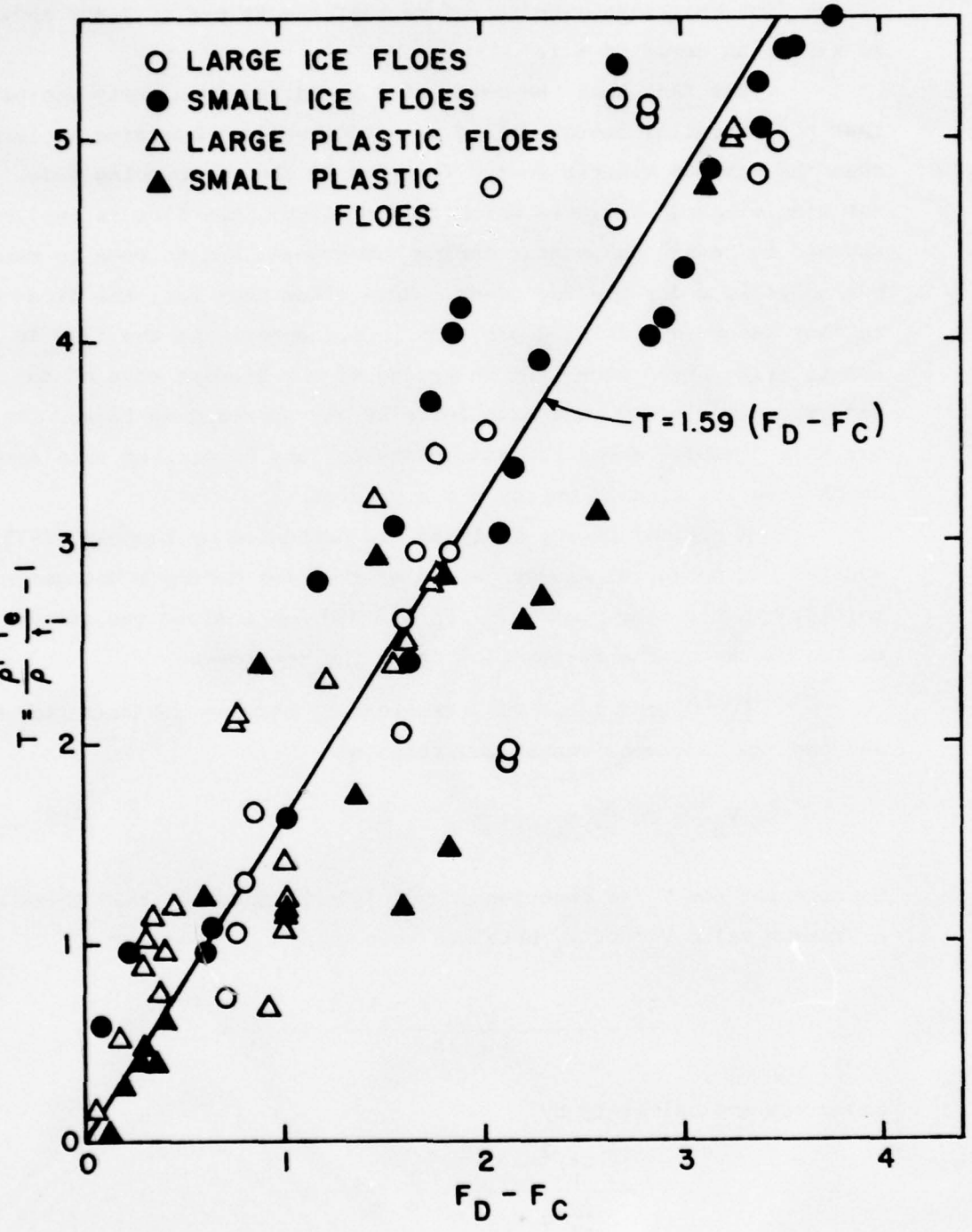

Figure 16. Dimensionless Ice Jam Thickness T as a Function of $(F_D - F_C)$

of one floe thickness, and therefore that the values of T are known only to within an error of $\pm$ 1.

The fact that the value of β is larger than unity indicates that the potential energy gained by a floe while submerging is larger than the maximum kinetic energy imparted by the surrounding flow. In the simple energy analysis which led to (II-8), the floe is implicitly assumed to remain horizontal during submergence and to come to rest horizontally under the ice cover. More often than not, the floes will in fact assume an inclined position. Furthermore, as the floe is submerged and is transported along the underside of the leading edge of the jam, it is subjected to a drag force by the surrounding flow. The floe may then "tumble" along the jam underside, and be carried to a larger depth than its kinetic energy would predict.

A similar energy analysis was presented by Kennedy (1975), who equated the potential energy gained by the floe during submergence to its initial kinetic energy $\rho' \forall V_n^2/2$, and did not include the energy imparted to the blocks by the faster flow under the ice cover.

D. Discussion. The relationship between the mean flow velocity and the jam thickness can be rewritten as

$$V_n^2 = 2g \frac{\Delta\rho}{\rho'} t_i \left[\frac{1}{\beta}\left(\frac{\rho'}{\rho}\frac{t_e}{t_i} - 1\right) + F_C\right] \left(1 - \frac{\rho'}{\rho}\frac{t_e}{t_i}\right)^2 \qquad \text{(II-9)}$$

Considering now V_n as function of $\frac{t_e}{h_n}$, (II-9) indicates that there exists a maximum value V_n^* of V_n obtained when

$$\frac{t_e}{h_n} = \frac{1 - 2\, t_i/h_n (1 - \beta F_C)}{3\ \rho'/\rho} \simeq \frac{\rho}{3\rho'} \simeq 0.36 \qquad \text{(II-10)}$$

and given approximately by

$$\frac{\left(\frac{2}{3} V_n^*\right)^2 - V_c^2}{2\frac{\Delta\rho}{\rho'} g\, t_i} = \frac{1}{\beta}\left(\frac{h_n}{t_i} - 1\right) \qquad \text{(II-11)}$$

The curves V_n versus t_e/h_n for the experimental conditions investigated with real ice floes are plotted in figure 17, where the experimental data are indicated and show good agreement with the calculated values. The

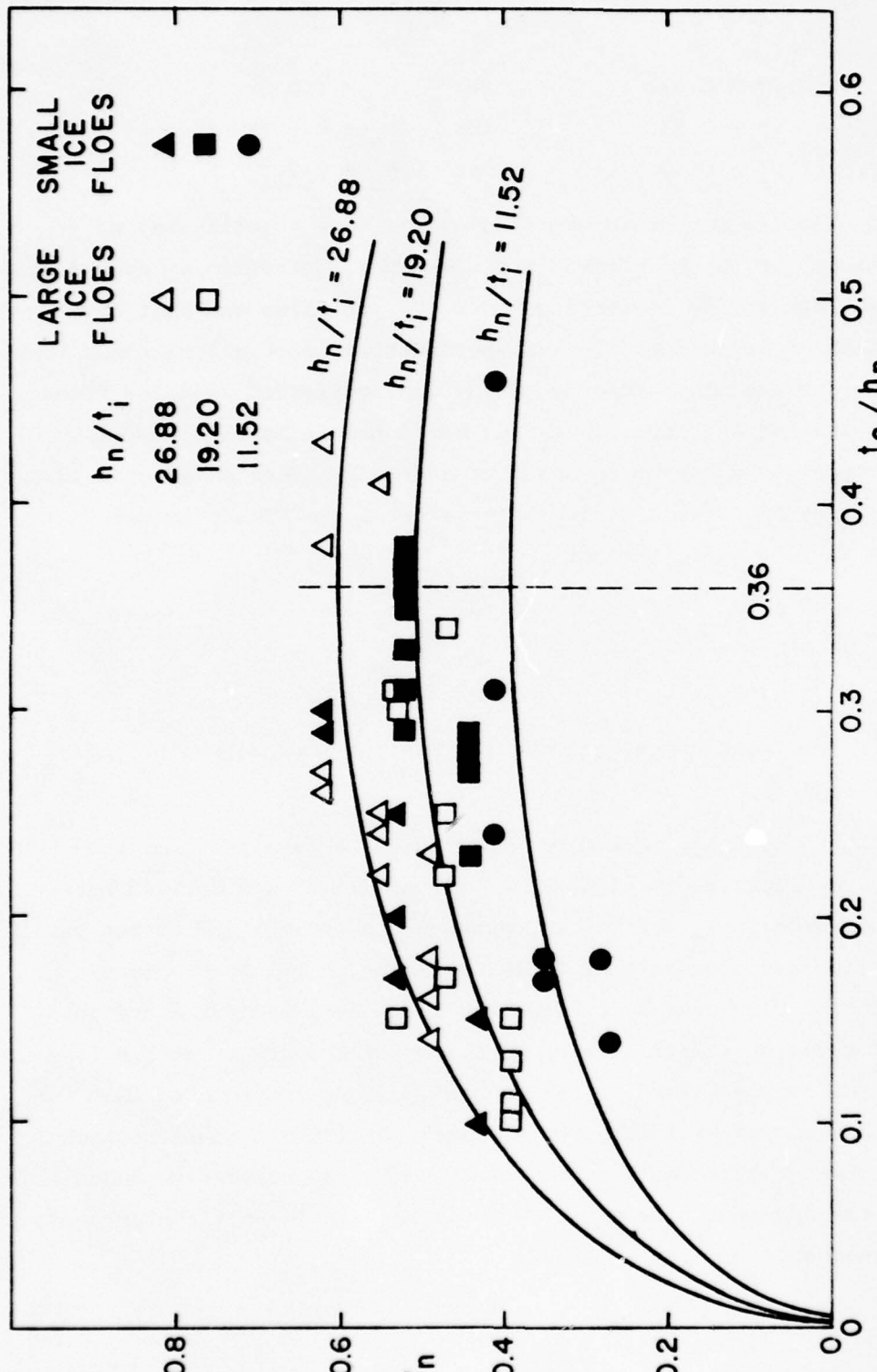

Figure 17. - Relationship between V_n and t_e/h_n for Present Experimental Conditions

calculated values of the maximum V_n for the three depths of flow studied are

$$V_n^* = 0.39 \quad \text{for} \quad h_n = 0.3 \text{ ft}$$
$$V_n^* = 0.51 \quad \text{for} \quad h_n = 0.5 \text{ ft}$$
$$V_n^* = 0.60 \quad \text{for} \quad h_n = 0.7 \text{ ft}$$

The maximum velocity can be interpreted as the flow velocity beyond which no stable jam can be formed in the channel. At velocity higher than the maximum value a floe is carried under the ice cover and past the screen instead of being deposited on the underside of the ice cover, therefore the ice jam cannot progress upstream and is limited to a few floes accumulated against the screen. As was mentioned in Section II-C-2, this phenomenon was observed to occur at a Froude number of about 0.13 when natural ice floes were used. This value of the Froude number corresponds to flow velocities of

$$V_n = 0.40 \quad \text{for} \quad h_n = 0.3 \text{ ft}$$
$$V_n = 0.52 \quad \text{for} \quad h_n = 0.5 \text{ ft}$$
$$V_n = 0.62 \quad \text{for} \quad h_n = 0.7 \text{ ft}$$

which are in excellent agreement with the maximum possible values of V_n predicted by (II-9).

E. Conclusion. Based on a simple energy analysis for floe submergence, a relationship given by (II-8) or (II-9) was derived between the approach velocity V_n and the thickness of the stable jam formed purely by accumulation and transport of floes. This relationship predicts a maximum relation thickness h_e/t_n equal to $\rho/3\rho'$ attained for a critical velocity V_n^* given by (II-11). When V_n is larger than V_n^* no stable fragmented ice jam can be formed in the channel. It is conjectured that for $V_n > V_n^*$ either no jam will form, or if blockage of the channel section occurs a backwater curve will form increasing the approach flow depth and decreasing the approach flow velocity until new stable equilibrium conditions are reached.

III. COMPRESSIVE STRENGTH OF FLOATING FRAGMENTED ICE COVERS

A. Introductory Remarks. It was mentioned in the Foreword that the thickness of a jam initially is determined by the depth to which arriving floes can be submerged, and subsequently by the internal collapse of the jam that occurs when the loading at a section exceeds the strength of the ice cover, either because of load increase or because the jam weakens. The increase in loading at a section may result from increase in the length of the jam upstream from the section, increase in water discharge, streamwise winds, etc. The strength of a jam will weaken as a result of partial thawing when air temperature rises. Recently, Uzuner and Kennedy (1974) developed an analytical model for the equilibrium thickness, t, of ice associated with internal failure of the ice cover. Their analysis requires an estimation of the longitudinal normal strength, σ_{cr}, of the floating fragmented ice cover, or equivalently of the streamwise stress coefficient, k_x, which is the ratio of σ_{cr} to the average vertical stress over the jam thickness, $\bar{\sigma}_z$, and which is proportional to σ_{cr}/t. In the original tests conducted by Uzuner for the determination of σ_{cr} it appeared that the covers tested were too long and that much of the compressive load applied to the cover specimen was transferred to the walls of the experimental tank thorugh shear, and consequently the observed failures might have been due at least partially to shear. Furthermore, a buckling type of failure was observed to occur at times, which was believed to be an artifact of the laboratory test apparatus and which likely does not occur in most field situations. Consequently, a new series of experiments was undertaken using shorter covers and regularly shaped ice blocks of various sizes.

B. Experimental Set-up and Procedure. 1. Experimental unit. The experiments to determine the compressive strength of fragmented ice covers were conducted in the 20-foot long, 3-foot wide, and 2-foot deep insulated force tank of the Institute's Low Temperature Flow Facility. The compression apparatus consisted of a driving plate attached to a variable speed carriage through a moment-insensitive dynamometer; the setup is depicted schematically in figure 18. The carriage was supported by four ball-bushings which rode on one-inch diameter rails affixed to the

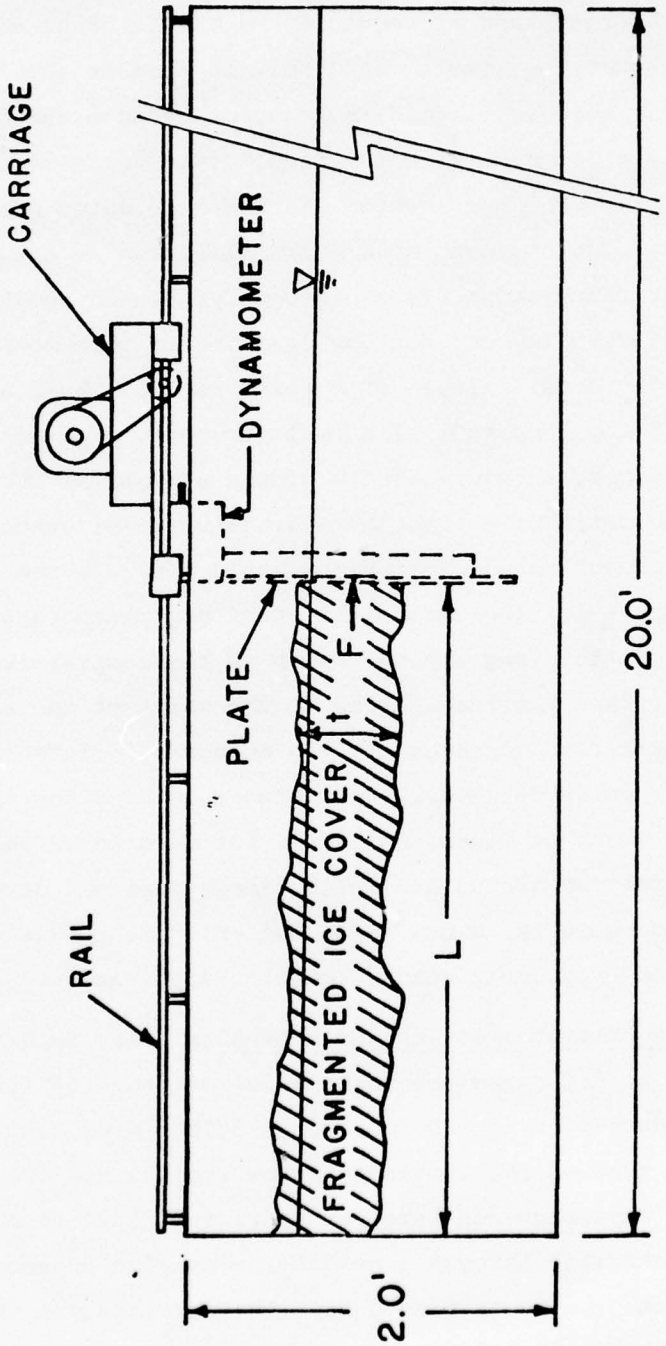

Figure 18. Sketch of Experimental Apparatus for Study of Compressive Strength of Fragmented Ice Cover

top of the walls of the force tank. It was driven by a variable speed, one-horsepower, DC motor through a cone-pulley system, geared speed reducer, two pinion gears at the end of the drive shaft extending across the tank, and a rack affixed to the top of each long wall of the flume. The motor speed was remotely controlled through a SCR drive control; the carriage velocity could be varied from 0.004 cm/sec to 2.4 cm/sec. The force sensing element of the dynamometer was composed of Statham Universal load cell, Model UL4, and transducing cell, Model UC3, referred to collectively as the force transducer. The load limit of the load cell was 200 pounds. The voltage output of the force transducer was amplified by and recorded on a mulitple channel Beckman Dynograph Type 504A. The force measuring system was calibrated by applying known horizontal loads to the driving plate and was found to be linear with calibration constants of 11.48 lb/mv, 11.42 lb/mv, and 11.05 lb/mv for recorder sensitivities of 2 mv/cm, 1 mv/cm, and 0.5 mv/cm, respectively.

The displacment of the driving plate was measured by a 10-turn potentiometer attached to the carriage and driven by a small rubber wheel in contact with one of the rails supporting the carriage. The potentiometer was calibrated, and its voltage output was recorded during each test on a second channel of the Dynograph recorder. The carriage velocity could be then determined accurately from the displacement-time record, and its constancy verified.

2. Test materials. Three different sizes of ice blocks were used in the experiments: commercial ice cubes (1.38 in. × 1.38 in. × 1.38 in.) and the two sizes of rectangular ice blocks made in the IIHR ice-maker and used in the ice-jam studies reported in Sections I and II (1 1/2 in. × 1 1/4 in. × 5/16 in., and 3 in. × 2 1/2 in. × 5/16 in.). The effective plan dimension, d_e, of a floe was defined by

$$d_e = \frac{b}{d} \left(\frac{d+b}{2}\right)$$

where d and b are the larger and smaller plan dimensions of a block, respectively. The values of d_e for the three types of ice floes used are

d_e = 1.0 in. for the ice cubes

d_e = 1.15 in. for the smaller ice parallelepipeds

d_e = 2.29 in. for the larger ice parallelepipeds

3. Experimental procedure. The experimental procedure followed in each compression test was as follows: The thermostat in the room was set at 0°C and the water in the tank was allowed to reach this temperature. The required quantity of ice blocks then was placed in front of the driving plate in the tank to obtain the required cover length, L, and thickness, t. The floating cover was gently agitated with a plastic rod to insure uniform thickness throughout the cover and homogeneous distribution of the ice blocks. The cover thickness was measured by means of a staff gage fitted with a scale and a 3 in. by 5 in. plate attached perpendicularly to the staff. The gate was inserted through the ice cover, whose thickness was determined from the scale attached to the gage staff. The carriage was set in motion at a predetermined speed and the voltage output of the force transducer and displacement potentiometer were recorded versus time on a Dynograph chart. Since the shape of the ice floes would be altered by interparticle friction, chipping under compression, melting, etc., the floes were replaced frequently during any series of tests.

C. Presentation of Results and Discussion. Typical examples of force-time records are shown in figure 19. It is seen that the force exerted on the driving plate initially increased almost linearly, reached a first maximum, and then dropped abruptly; this indicated failure of the fragmented ice cover under compression. When the compression process was continued further, the force started increasing again until a new peak was reached and the ice cover failed again. This indicated that after the initial failure, the individual ice floes in the fragmented ice cover rearranged themselves and the cover recovered its strength. The first force maximum recorded on the force-time record was taken as the failure strength for the initial ice cover of length L and thickness t, for the selected speed of application of the load, V_c. However, considerable variation in the failure force was observed between nominally identical tests (same ice blocks, same values of L, t, and V_c). This variation in in the cover strength is attributable to variation in

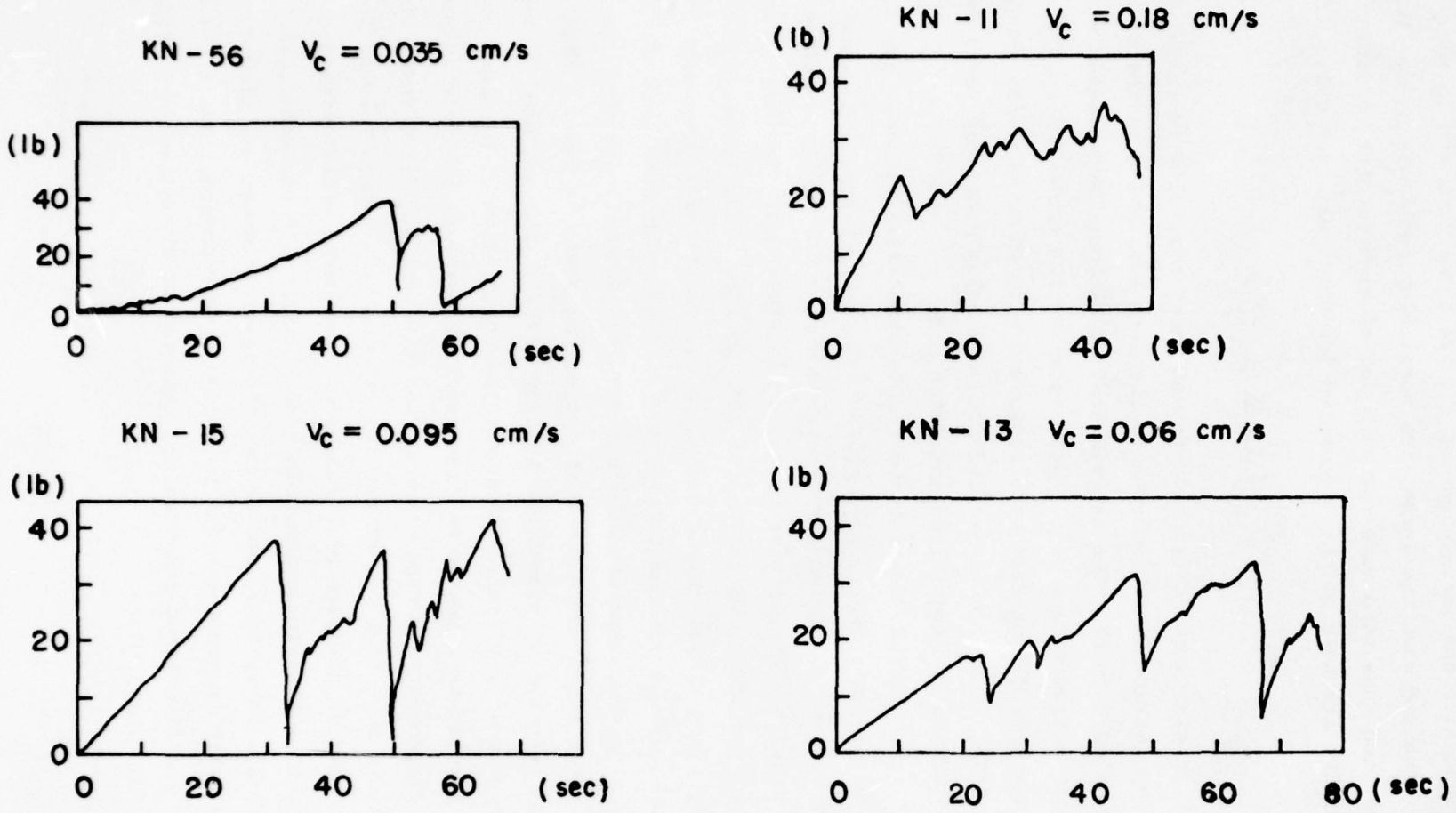

Figure 19. Typical Force-vs-Time Records Obtained in Compression Tests of Fragmented Ice Covers

the orientation and arrangement of the ice floes from run to run. It was more pronounced when the larger ice parallelepipeds were used. Therefore, at least ten runs were made for each set of experimental conditions. The compressive strength of the fragmented ice cover was then defined as

$$\sigma_{cr} = \frac{\frac{1}{n}\sum_{i=1}^{n} F_i}{Wt}$$

where n is the number of runs performed under nominally identical conditions, F_i is the failure force recorded in the i-th run, and W is the width of the ice cover (3.0 feet). The experimental conditions investigated and corresponding measured values of σ_{cr} are listed in the tables of Appendix D. Tests numbered PG1 to PG24 were performed with commercial ice cubes, tests numbered KN1 to KN43 with smaller ice parallelepipeds, and tests numbered KN44 to KN64 with larger ice parallelepipeds.

From the force-time and displacement-time records, the longitudinal normal stress, σ_x, experienced by the ice cover at any time T, and the corresponding strain, E, defined as $\Delta L/L$, where $\Delta L = V_c T$ is the distance traveled by the driving plate at time T, could be determined. Typical stress-strain curves are shown in figures 20a and 20b. Each figure depicts three representative curves corresponding to different carriage speeds for the same ice-cover length and thickness. It can be observed that the yield stress, σ_{cr}, decreases with increasing plate velocity and that the strain at the yield point decreases with increasing plate velocity. This phenomenon has been reported by Uzuner and Kennedy (1974), who explained it in terms of a supercooling effect. In short, the application of pressure on fragmented ice blocks leads to melting and refreezing at particle interfaces, with the accompanying production of cohesive welds. Since lower strain rate allows more time for refreezing and thus for cohesive bonds to develop, the compressive strength of a fragmented ice cover will increase with decreasing rate of deformation. In some of the tests performed, listed as PG-7, PG-19, KN-1, KN-7, and KN-34, the carriage speed was slow enough for theoriginally fragmented cover to become, under compression, a solid cover, and the yielding force exceeded the capacity of the dynamometer transducer system (200 lbs).

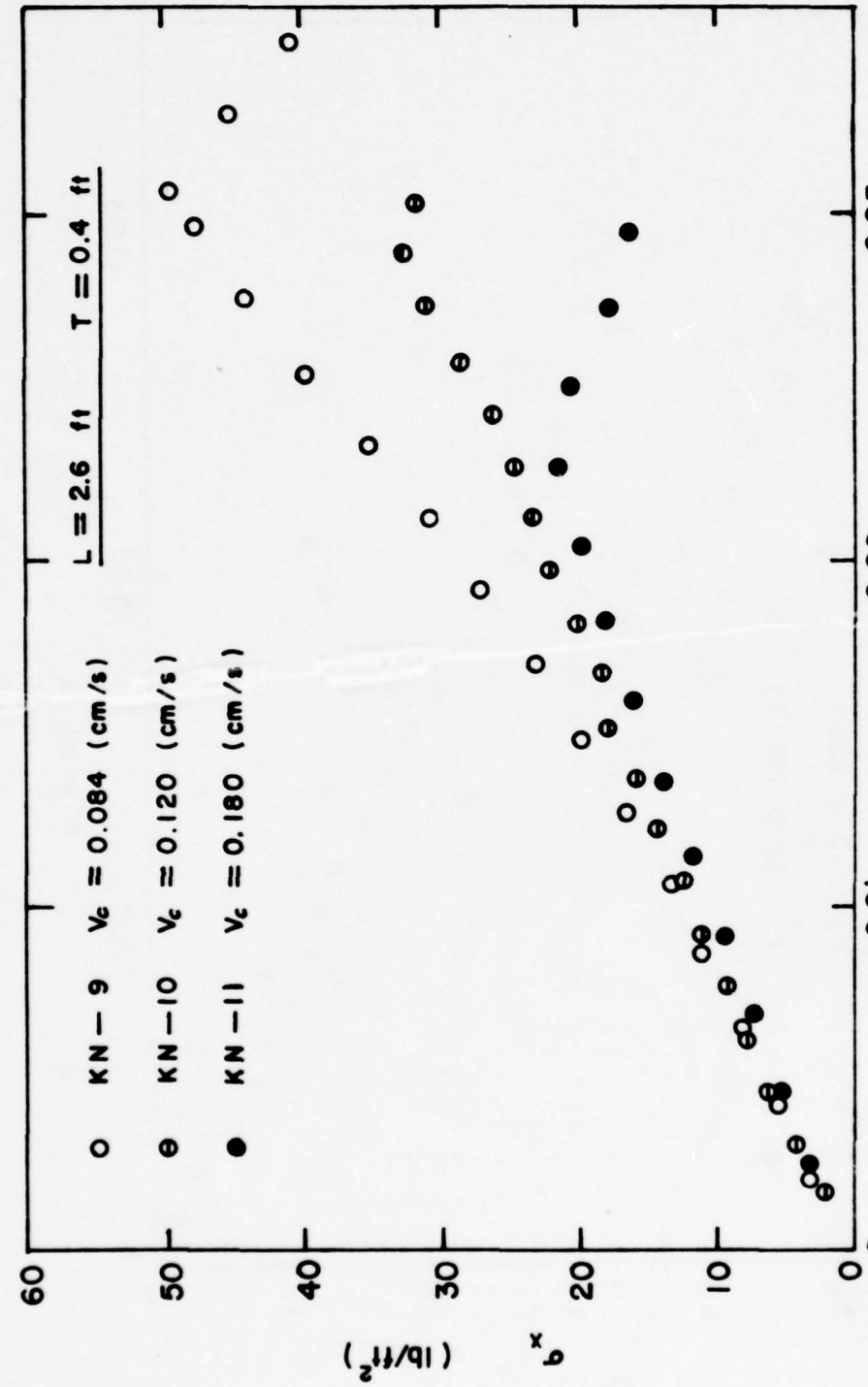

Figure 20. Compressive Strength of Fragmented Ice Covers - Typical Stress-Strain Curves Obtained with Small Ice Farallelepipeds

a) L = 2.6 ft, t = 0.4 ft

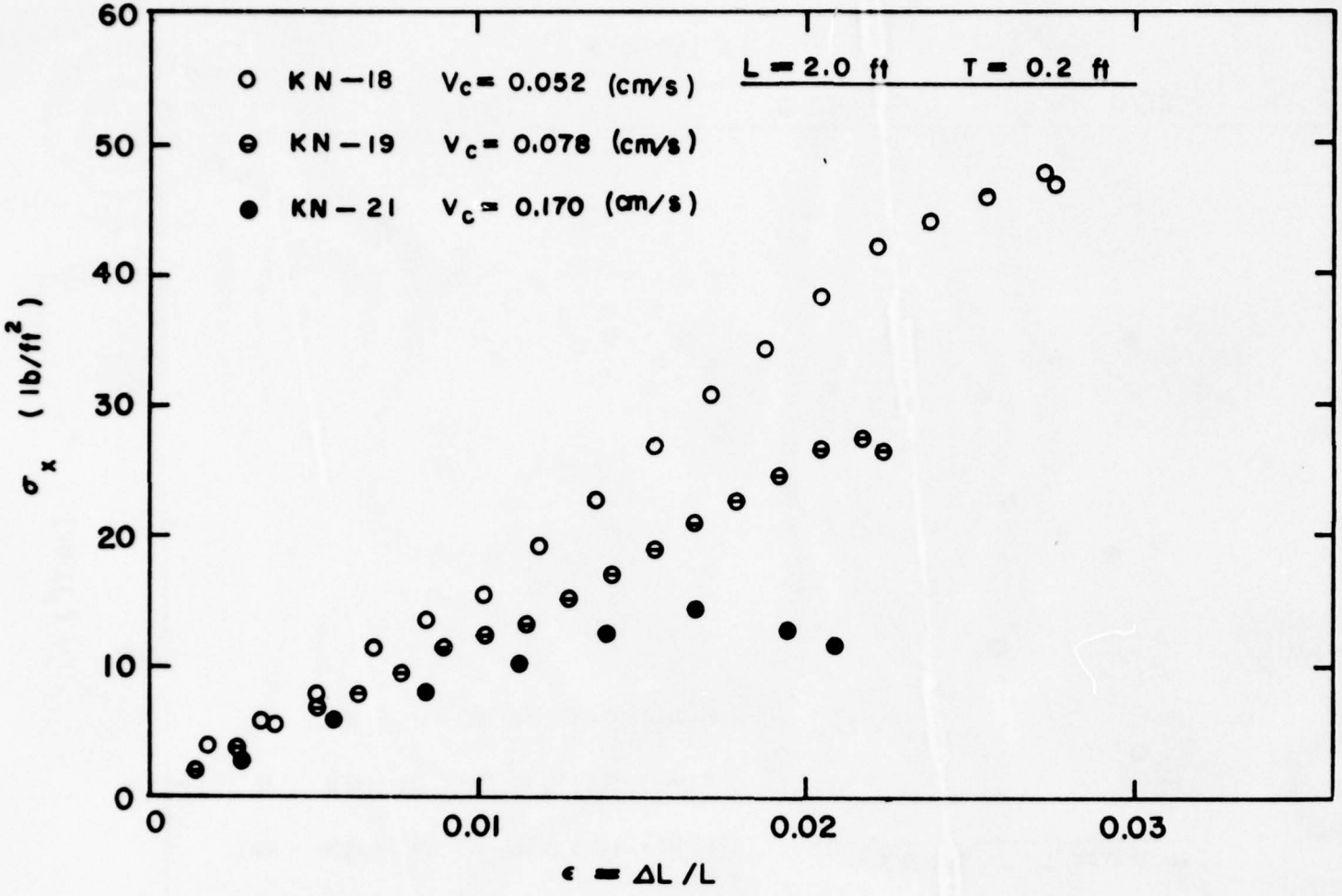

Figure 20. Compressive Strength of Fragmented Ice Covers - Typical Stress-Strain Curves Obtained with Small Ice Parallelepipeds

b) L = 2 ft, t = 0.2 ft

The results of the compression tests are plotted for the three floe sizes used in the experiments as compressive strength corresponding to the first failure, σ_{cr}, versus plate velocity, V_c, in figure 21, and as σ_{cr}/t, which is proportional to the streamwise stress coefficient, k_x, defined by Uzuner and Kennedy (1974), versus V_c in figure 22. In both figures, the majority of the data points fall on or around a straight line with slope of -1 on the log-log plots. It appears, therefore, that the compressive strength of fragmented ice covers is inversely proportional to the compression velocity V_c, but is independent of the cover length and floe shape or size. Since the ice cover subjected to compression is fragmented, it can be expected that the force applied by the driving plate at the loaded end of the cover is transmitted to other sections of the cover only after sufficient compaction of the ice floes has occurred, and that therefore the stress experienced at sections along the cover length decreases rapidly with distance from the plate. During the experiments it was indeed observed that the failure zone always was located within a short distance from the driving plate; no specific measurements of the distance from the plate at which failure first occurred were made. The apparent independence of σ_{cr} from floe size and shape is more unexpected. All attempts at finding systematic variation of σ_{cr} with relative jam thickness parameters such as t/d_e or t/t_i, where t_i is the floe thickness, were unsuccessful. It is possible that the ranges of floe size and jam thickness investigated were insufficient for the effect of relative jam thickness to be distinguished within the experimental scatter inherent to this type of study.

D. Conclusion. The results of the study on compressive strength of floating fragmented ice cover may be summarized as follows.

1. The failure strength, σ_{cr} is inversely proportional to the velocity of the driving plate V_c,

$$\sigma_{cr} = K V_c^{-1}$$

2. The compressive strength of a fragmented cover is independent of length cover L.

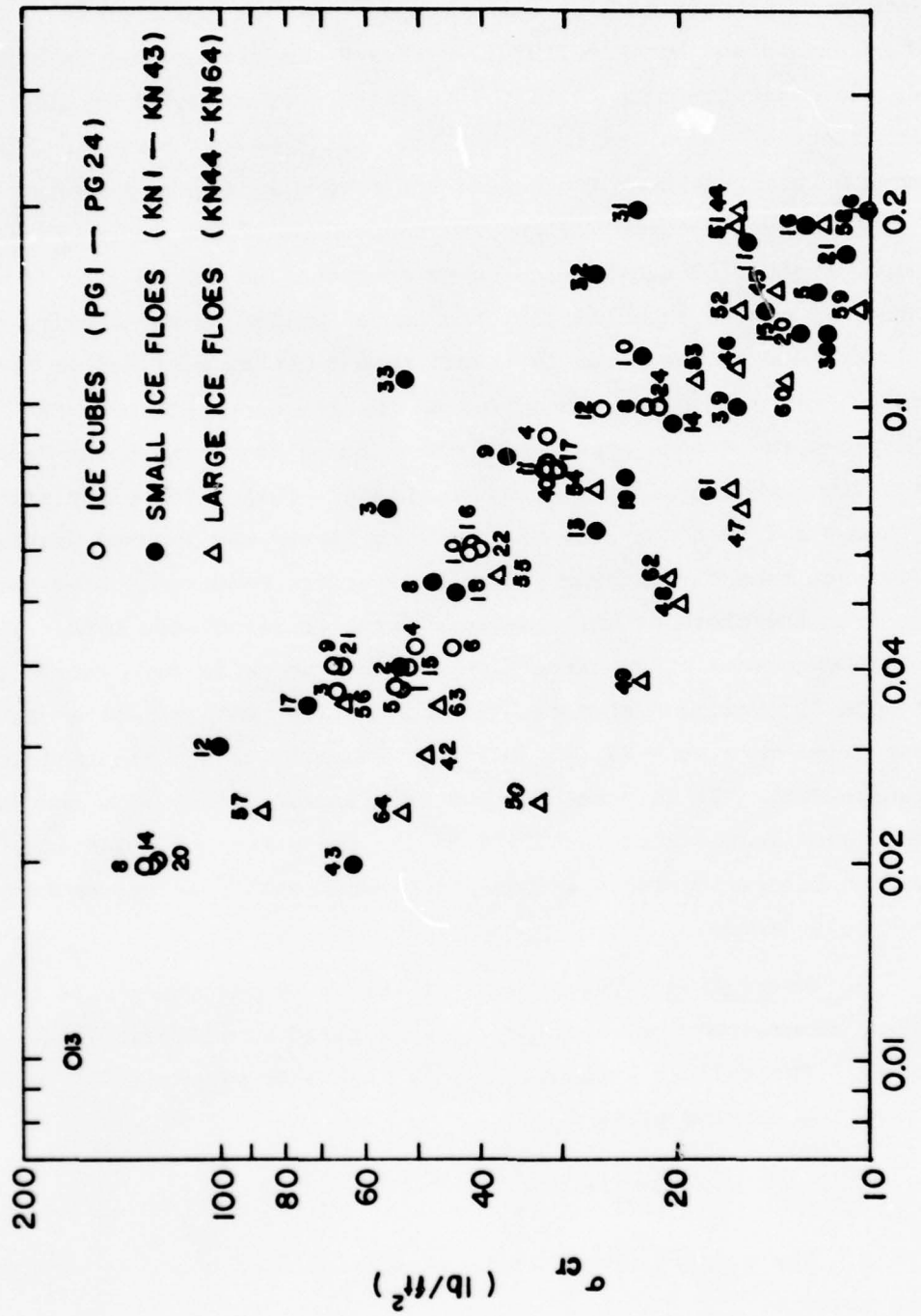

Figure 21. Compressive Strength of Fragmented Ice Covers versus Plate Velocity V_c

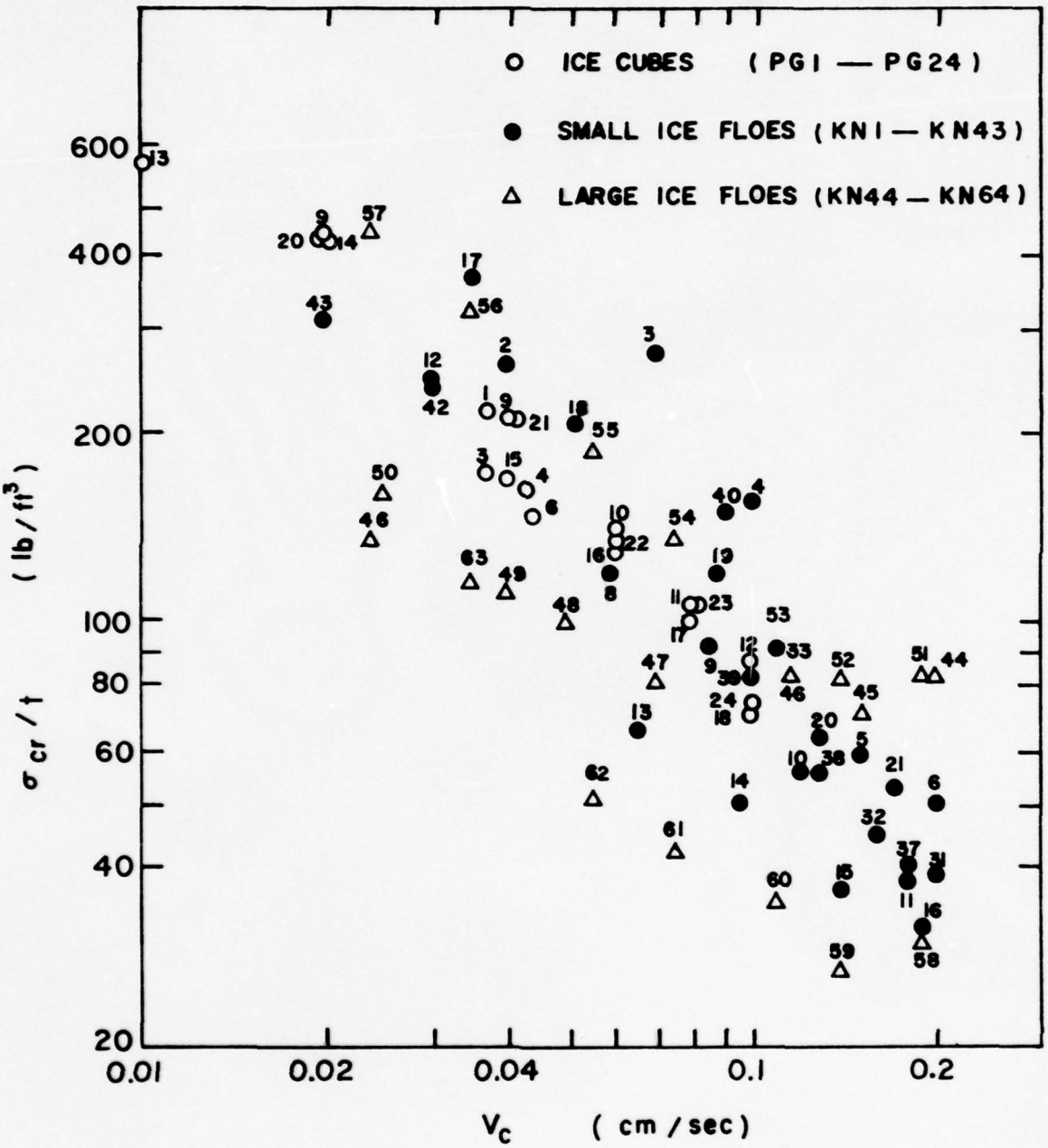

Figure 22. Ratio of Compressive Strength to Ice Cover Thickness versus Plate Velocity V_c

3. Further experiments covering a wider range of jam thickness and floe sizes are necessary to clarify the effect of relative jam thickness and floe geometry on the compressive strength σ_{cr}.

REFERENCES

Ashton, G.D. (1974), "Froude Criterion for Ice-Block Stability," Journal of Glaciology, Vol. 13, No. 68, pp. 309-313.

Calkins, D.J., and Ashton, G.D. (1975), "Arching of Fragmented Ice Covers," Special Report 222, Cold Regions Research and Engineering Laboratory, Hanover, New Hampshire.

Kennedy, J.F. (1975), "Ice Jam Mechanics," Proceedings, Third International Symposium on Ice Problems, Hanover, New Hampshire, pp. 143-164.

Michel, B. (1957), "Etude de l'Entrainement des Glacons sous un Couvert de Glace," Report No. 108, Laboratoire d'Hydraulique LaSalle, Quebec, Canada.

Pariset, E., Hausser, R., and Gagnon, A. (1966), "Formation of Ice Covers and Ice Jams in Rivers," Proc. ASCE, Journal of Hydraulic Division, Vol. 92, HY6.

Uzuner, M.S., and Kennedy, J.F. (1974), "Hydraulics and Mechanics of River Ice Jams," IIHR Report No. 161, Iowa Institute of Hydraulic Research, The Univ. of Iowa, Iowa City, Iowa.

Wu, S. (1971), "Calculation of Interfacial Tension in Polymer Systems," Journal of Polymer Science, Part C, No. 34.

APPENDIX A

Experimental Results on Ice Jam Initiation

Note: In the following tables, the formation of a stable arch across the channel constriction is indicated by the symbol O. No arching is indicated by the symbol X.

In the experiments on ice-jam initiation the approach flow depth was kept constant, h_n = 0.5 feet. When real ice floes were used, due to partial melting the ratio h_n/t_i was found to vary between 19 and 21, approximately.

Table A1 - Ice Jam Initiation Experiments with Small Ice Floes
($1\frac{1}{2}$ in x $1\frac{1}{4}$ in x 5/16 in)

Exp. No.	B	W	Q_i	Q_w	V_n	L/B	B/W	F_r	C_g	C	
	ft	ft	cfs	cfs	fps						
IB1	.667	1.000	.0026	.121	.241	.187	.667	.060	.515	.344	O
2			.0015						.316	.211	X
3			.0019						.405	.270	X
4			.0022						.462	.308	X
5			.0030						.659	.439	O
6			.0022						.491	.327	O
7		1.333	.0035	.161	.241		.500		.703	.351	O
8			.0023						.460	.230	O
9			.0019						.384	.192	X
10			.0025						.528	.264	O
11		1.600	.0026	.193	.241		.417		.524	.218	X
12			.0031						.636	.265	O
13			.0027						.555	.232	O
14			.0036						.713	.297	O
15			.0016						.331	.138	X
16			.0026						.532	.222	O
17			.0021						.440	.183	X
18			.0021						.449	.187	X
19		2.000	.0027	.241	.241		.333		.533	.178	O
20			.0021						.417	.139	X
21			.0024						.497	.165	O
22	.500	1.433	.0024	.173	.241	.250	.349		.645	.225	O
23			.0020						.541	.189	X
24			.0020						.571	.199	O
25			.0016						.452	.158	O
26			.0015						.439	.153	X
27		1.000	.0015	.121	.241		.500		.408	.204	X
28			.0019						.504	.252	O
29			.0024						.653	.326	O

Table A1 - continued

Exp. No.	B ft	W ft	Q_i cfs	Q_w cfs	V_n fps	L/B	B/W	F_r	C_g	C	
30			.0016						.439	.219	X
31		.833	.0017	.100	.241		.600		.460	.276	O
32			.0013						.346	.207	X
33			.0015						.410	.246	X
34			.0017						.458	.275	O
IF1	.333	2.00	.0085	.340	.340	.375	.167	.084	2.419	.404	O
2			.0044						1.263	.211	O
3			.0014						1.407	.068	X
4			.0019						.557	.093	O
5			.0034	.384	.384			.095	.868	.145	O
6			.0023						.599	.100	X
7			.0029						.718	.120	O
8			.0019						.509	.085	X
9			.0028						.742	.124	O
10			.0039	.425	.425			.105	.874	.146	O
11			.0032						.736	.123	X
12			.0038						.862	.144	X
13			.0044						1.024	.171	O
14			.0040					.115	.952	.159	O
15			.0067	.465	.465			.115	1.377	.230	O
16			.0071						1.467	.245	O
17			.0069						1.455	.243	X
18			.0085						1.808	.302	O
19			.0046						.988	.165	X
20			.0105	.506	.506			.125	2.072	.346	O
21			.0115						2.203	.368	O
22			.0085						1.647	.275	X
23			.0051						1.012	.169	X
24			.0061						1.215	.203	X
25			.0082						1.670	.279	O

Table A1 - continued

Exp. No.	B ft	W ft	Q_i cfs	Q_w cfs	V_n fps	L/B	B/W	F_r	C_g	C	
26			.0063						1.287	.215	O
27			.0126	.551	.551			.135	2.269	.379	O
28			.0109						2.000	.334	X
29			.0072						1.347	.225	X
30			.0094						1.695	.283	O
31			.0098						1.785	.298	O
32			.0064						1.144	.191	X
33			.0082						1.461	.244	O
34			.0106	.578	.578			.145	1.760	.294	X
35	.333	2.00	.0136	.578	.578	.375	.167	.145	2.287	.382	O
36			.0109						1.868	.312	X
37			.0160	.600	.600			.147	2.587	.432	O
38			.0113						1.856	.310	X
39			.0161						2.683	.448	O
40			.0132						2.215	.370	X
41			.0141	.618	.618			.155	2.239	.374	X
42			.0192						3.305	.552	X
43			.0162	.642	.642			.157	2.544	.425	X
44			.0206						3.114	.520	X
45			.0231						3.503	.585	O
46			.0213						3.227	.539	X
47			.0251						3.850	.643	O
48			.0243	.672	.672			.168	3.455	.577	X
49			.0175						2.509	.419	X
50			.0261	.694	.694			.170	3.730	.623	X
51			.0010	.281	.281			.070	.359	.060	X
52			.0005						.174	.029	O
53			.0008						.257	.046	X
54			.0005						.197	.033	O

Table A1 - continued

Exp. No.	B	W	Q_i	Q_w	V_n	L/B	B/W	F_r	C_g	C	
	ft	ft	cfs	cfs	fps						
55			.0004	.200	.200			.050	.197	.033	O
56	.500	2.00	.0054	.345	.345	.250	0.250	.098	.920	.230	O
57			.0038						.668	.167	O
58			.0024						.428	.107	X
59			.0024						.448	.112	X
60			.0034						.652	.163	O
61			.0047	.384	.384			.110	.712	.178	X
62			.0061						.940	.235	O
63			.0051						.792	.198	X
64			.0054						.840	.210	O
65			.0057						.900	.225	O
66			.0062	.419	.419			.120	.856	.214	X
67			.0096						1.348	.337	O
68			.0093						1.332	.333	O
69	.500	2.000	.0071	.419	.419	.250	.250	.120	1.028	.257	X
70			.0091						1.328	.332	O
71			.0126	.454	.454			.130	1.620	.405	O
72			.0143						1.864	.466	O
73			.0113						1.480	.370	O
74			.0083						1.100	.275	X
75			.0092						1.232	.308	X
76			.0142	.489	.489			.140	1.704	.426	X
77			.0217						2.688	.672	X
78			.0277						3.540	.885	X
79			.0251						3.008	.752	O
80			.0254						3.092	.773	O
81			.0178						2.208	.552	X
82			.0246	.524	.524			.150	2.744	.686	X
83			.0293						3.264	.816	X

Table A1 - continued

Exp. No.	B ft	W ft	Q_i cfs	Q_w cfs	V_n fps	L/B	B/W	F_r	C_g	C	
84			.0308						3.448	.862	X
85	.667	2.000	.0064	.323	.323	.187	.333	.082	.936	.312	O
86			.0057						.852	.284	O
87			.0049						.744	.248	O
88			.0039						.618	.206	O
89			.0026						.396	.132	X
90			.0036						.558	.186	O
91			.0034						.534	.178	X
92			.0032						.501	.167	X
93			.0037	.370	.370			.094	.471	.157	X
94			.0064						.825	.275	O
95			.0049						.642	.214	X
96			.0059						.795	.265	X
97			.0069						.930	.310	O
98			.0067						.924	.308	O
99			.0023	.400	.400			.099	2.763	.921	O
100			.0020						2.532	.844	O
101			.0146						1.827	.609	O
102			.0102						1.302	.434	O
103	.667	2.00	.0058	.398	.398	.187	.333	.099	.708	.236	O
104			.0068						.828	.276	O
105			.0039						.477	.159	X
106			.0049						.498	.166	X
107			.0054						.669	.223	X
108			.0078						.969	.323	O
109			.0053						.672	.224	X
110			.0061						.765	.255	O
111			.0119	.440	.440			.110	1.305	.435	O
112			.0083						.909	.303	X

Table A1 - continued

Exp. No.	B	W	Q_i	Q_w	V_n	L/B	B/W	F_r	C_g	C	
	ft	ft	cfs	cfs	fps						
113			.0102						1.134	.378	X
114			.0130						1.449	.483	O
115			.0151						1.689	.563	O
116			.0060						.654	.218	X
117			.0071						.792	.264	X
118			.0104						1.185	.395	O
119			.0104						1.218	.406	O
120			.0084						1.002	.334	X
121			.0108	.483	.483			.120	1.083	.361	O
122			.0106						1.098	.366	X
123			.0134						1.431	.477	X
124			.0189						2.082	.694	X
125			.0199						1.986	.662	O
126			.0150						1.509	.503	O
127			.0160						1.629	.543	X
128			.0121	.526	.526			.130	1.116	.372	X
129			.0154						1.455	.485	X
130			.0204						1.986	.662	X
131			.0217						2.163	.721	X
132			.0224						2.058	.686	X
133			.0258						2.424	.808	X
134			.0013	.281	.281			.070	.228	.076	X
135			.0020						.357	.119	X
136			.0034						.612	.204	O
137	.667	2.00	.0026			.187	.333	.070	.465	.155	O
138			.0018	.201	.201			.050	.444	.148	O
139			.0017						.411	.137	O
140			.0008						.207	.069	O
141			.0004						.108	.036	X

Table A1 - continued

Exp. No.	B ft	W ft	Q_i cfs	Q_w cfs	V_n fps	L/B	B/W	F_r	C_g	C	
142			.0007						.192	.064	O
143			.0006	.120	.120			.030	.255	.085	O
144			.0003						.144	.048	O
145	.833	2.00	.0053	.343	.343	.150	.417	.091	.568	.237	O
146			.0039						.427	.178	X
147			.0050						.554	.231	X
148			.0057						.628	.262	O
149			.0049						.549	.229	X
150			.0054						.611	.255	O
151			.0079	.375	.375			.100	.777	.324	O
152			.0066						.657	.274	X
153			.0078						.782	.326	X
154			.0093						.949	.396	O
155			.0083						.856	.357	O
156			.0100	.412	.412			.110	.962	.401	O
157			.0085						.770	.321	X
158			.0095						.873	.364	X
159			.0101						.940	.392	X
160			.0142						1.350	.563	X
161			.0114						1.017	.424	O
162			.0120						1.082	.451	O
163			.0095						.856	.357	X
164			.0107	.453	.453			.120	.871	.363	X
165			.0147						1.195	.498	X
166			.0180						1.457	.607	O
167			.0254						2.059	.858	X
168			.0174						1.389	.579	X
169			.0200	.490	.490			.130	1.536	.640	X
170			.0234						1.757	.732	X

Table A1 - continued

Exp. No.	B	W	Q_i	Q_w	V_n	L/B	B/W	F_r	C_g	C	
	ft	ft	cfs	cfs	fps						
171	.833	2.00	.0286	.490	.490	.150	.417	.130	2.148	.895	X
172			.0179						1.344	.560	X
173			.0222	.484	.484			.120	1.776	.740	X
174			.0202						1.620	.675	X
175			.0010	.201	.201			.050	.185	.077	X
176			.0023						.446	.186	O
177			.0019						.374	.156	O
178			.0013						.266	.111	X
179			.0042	.281	.281			.070	.575	.240	O
180			.0019						.261	.109	X
181			.0024						.340	.142	X
182			.0032						.465	.194	X
183			.0047						.693	.289	O
184			.0027	.321	.321			.08	.319	.133	X
185			.0053						.655	.273	O
186			.0043						.542	.226	X
187			.0056						.719	.300	O
188			.0058						.758	.316	O
189	1.33	2.00	.0111	.342	.342	.093	.667	.082	.804	.536	O
190			.0070						.418	.279	X
191			.0096						.712	.475	X
192			.0125						.937	.625	X
193			.0126						.940	.627	O
194			.0100						.756	.504	O
195			.0082						.630	.420	X
196			.0099	.389	.389			.0933	.630	.420	X
197			.0119						.760	.507	X
198			.0162						1.050	.701	X
199			.0187						1.222	.815	X

Table A1 - continued

Exp. No.	B ft	W ft	Q_i cfs	Q_w cfs	V_n fps	L/B	B/W	F_r	C_g	C	
200			.0203						1.344	.896	X
201			.0130	.360	.360			.086	.888	.592	O
202			.0079						.547	.365	X
203			.0102						.702	.468	X
204			.0169						1.168	.779	O
205	1.33	2.00	.0123						.858	.572	X
206			.0147						1.026	.684	X
207			.0108	.339	.339			.086	.759	.506	O
208			.0102						.723	.482	X
209			.0121						.874	.583	X
210			.0167						1.213	.809	X
211			.0115	.373	.373			.094	.733	.489	X
212			.0184						1.183	.789	X
213			.0101	.299	.299			.075	.808	.539	O
214			.0084						.679	.453	O
215			.0068						.559	.373	X
216			.0084						.690	.460	O
217			.0070						.580	.387	X
218			.0079						.630	.420	X
219			.0057	.264	.264			.066	.531	.354	X
220			.0071						.670	.447	O
221			.0063						.600	.400	O
222			.0022	.201	.201			.050	.267	.178	X
223			.0050						.601	.401	O
224			.0044						.538	.359	X
225			.0054						.669	.446	O
226			.0056	.160	.160			.040	.844	.563	O
227			.0043						.649	.433	O

Table A1 - continued

Exp. No.	B	W	Q_i	Q_w	V_n	L/B	B/W	F_r	C_g	C	
	ft	ft	cfs	cfs	fps						
228			.0028						.423	.282	O
229			.0021						.318	.212	X

Table A2 - Ice Jam Initiation Experiments with Large Ice Floes
(3 in x 2.5 in x 5/16 in)

Exp. No.	B	W	Q_i	Q_w	V_n	L/B	B/W	F_r	C_g	C	
	ft	ft	cfs	cfs	fps						
IF230	.667	2.000	.0017	.320	.320	.375	.333	.080	.276	.092	X
231			.0025	.400	.400			.100	.300	.100	X
232			.0047						.582	.194	O
233			.0039						.489	.163	X
234			.0048						.606	.202	O
235			.0078	.480	.480			.120	.783	.261	X
236			.0107						1.174	.358	X
237			.0133						1.353	.451	X
238			.0141						1.455	.485	O
239			.0007	.160	.160			.040	.216	.072	X
240			.0008						.249	.083	O
241			.0007						.222	.074	O
242			.0012	.240	.240			.06	.242	.081	X
243			.0013						.267	.089	O
244			.0010						.225	.075	X
245			.0024	.320	.320			.08	.363	.121	O
246			.0021						.318	.106	O
247			.0012						.195	.065	X
248	.833	2.00	.0029	.400	.400	.300	.417	.100	.273	.114	X
249			.0088						.842	.351	O
250			.0053						.513	.214	X
251			.0072						.693	.289	O
252			.0078						.749	.311	O
253			.0064						.616	.257	X
254			.0123	.480	.480			.120	.978	.408	X
255			.0147						1.173	.489	X
256			.0158						1.266	.528	O
257			.0118						.940	.392	X
258			.0065					.080	.782	.326	O

Table A2 - continued

Exp. No.	B ft	W ft	Q_i cfs	Q_w cfs	V_n fps	L/B	B/W	F_r	C_g	C	
259			.0032						.379	.158	O
260			.0019						.223	.093	X
261			.0023						.276	.115	X
262			.0013	.240	.240			.060	.213	.089	X
263			.0020						.324	.135	O
264	.833	2.00	.0017	.240	.240	.300	.417	.060	.271	.113	X
265			.0014	.160	.160			.040	.333	.139	O
266			.0011						.273	.114	O
267			.0009						.211	.088	X
268	1.33	2.00	.0026	.160	.160	.187	.667	.040	.390	.260	X
269			.0044						.672	.448	O
270			.0032						.496	.331	X
271			.0041						.639	.426	O
272			.0039						.624	.416	O
273			.0062	.240	.240			.060	.622	.415	O
274			.0046						.465	.310	X
275			.0043						.441	.294	X
276			.0062						.643	.429	X
277			.0073						.769	.513	O
278			.0052						.516	.344	O
279			.0050						.517	.345	X
280			.0056						.594	.396	X
281			.0044						.484	.323	X
282			.0038						.384	.256	X
283			.0053						.544	.363	X
284			.0056						.580	.287	X
285			.0037						.375	.250	X
286			.0081						.673	.449	X
287			.0062						.616	.411	X

Table A2 - continued

Exp. No.	B	W	Q_i	Q_w	V_n	L/B	B/W	F_r	C_g	C	
	ft	ft	cfs	cfs	fps						
288			.0100						1.002	.668	O
289			.0065	.320	.320			.080	.483	.322	X
290			.0081						.613	.409	X
291			.0082						.624	.416	X
292			.0117						.900	.600	O
293			.0108						.843	.562	O
294			.0141	.400	.400			.100	.841	.561	X
295			.0169						1.020	.680	X
296			.0181						1.107	.738	X

Table A3 - Ice Jam Initiation Experiments with Small Plastic Blocks
(1½ in x 1¼ in x 3/8 in)

Exp. No.	B	W	Q_i	Q_w	V_n	L/B	B/W	F_r	C_g	C	
	ft	ft	cfs	cfs	fps						
PB1	.500	1.433	.0010	.200	.281	.250	.349	.07	.193	.067	O
2			.0007						.129	.045	X
3		1.000	.0007	.140	.281		.500		.127	.063	X
4			.0017						.321	.160	O
5			.0010						.183	.091	O
6			.0008						.161	.080	O
7		.833	.0013	.117	.281		.600		.251	.152	O
8			.0007						.134	.081	X
9			.0011						.204	.122	O
10			.0006						.118	.071	X
11			.0009						.163	.098	X
12		2.00	.0026	.281	.281		.250		.494	.123	O
13			.0009						.174	.043	X
14			.0011						.220	.055	O
15			.0009						.181	.045	O
16	.667	1.00	.0010	.140	.281	.187	.667		.145	.096	X
17			.0014						.205	.137	X
18			.0034						.487	.325	O
19			.0021						.307	.205	O
20			.0023						.330	.220	X
21			.0026						.373	.249	O
22			.0023						.337	.224	O
23			.0016						.263	.175	O
24			.0014						.207	.138	X
25		1.333	.0024	.187	.281		.500		.336	.168	O
26			.0012						.176	.088	X
27			.0017						.240	.120	X
28			.0024						.337	.169	O
29		1.60	.0016	.225	.281		.417		.230	.096	O

Table A - continued

Exp. No.	B	W	Q_i	Q_w	V_n	L/B	B/W	F_r	C_g	C	
	ft	ft	cfs	cfs	fps						
30			.0018						.252	.105	X
31			.0031						.442	.184	O
32			.0023						.334	.139	O
33			.0016						.227	.095	X
34		2.00	.0019	.281	.281		.333		.270	.090	O
35	.667	2.00	.0015	.281	.281	.187	.333		.219	.073	X
36			.0023						.334	.111	O
37		1.00	.0016	.140	.281		.667	.06	.234	.156	X
38			.0013						.180	.120	X
39			.0019						.268	.179	O
40			.0023						.324	.216	O
41		1.33	.0026	.187	.281		.500		.378	.189	O
42			.0020						.280	.140	O
43			.0025						.360	.180	O
44			.0018						.256	.128	O
45			.0018						.260	.130	O
PF1	.667	2.00	.0018	.281	.281	.187	.333	.07	.258	.086	X
2			.0026						.376	.125	O
3			.0021						.294	.098	O
4			.0016						.228	.076	O
5			.0013						.185	.061	O
6			.0026						.366	.122	X
7			.0024	.361	.361			.09	.266	.090	X
8			.0018						.199	.066	O
9			.0026						.288	.098	X
10			.0020						.225	.075	O
11			.0046	.441	.441			.11	.417	.140	O
12			.0031						.281	.094	O
13			.0030						.272	.090	O

Table A3 - continued

Exp. No.	B	W	Q_i	Q_w	V_n	L/B	B/W	F_r	C_g	C	
	ft	ft	cfs	cfs	fps						
14			.0018						.163	.054	X
15			.0024						.217	.073	X
16			.0034	.522	.522			.13	.261	.087	O
17			.0031						.240	.080	X
18			.0036						.273	.091	X
19			.0046						.354	.118	O
20			.0034						.264	.088	X
21			.0052						.345	.115	O
22			.0055						.369	.123	O
23	.500		.0026	.281	.281	.250	.250	.07	.493	.123	O
24			.0009						.174	.044	X
25			.0011						.209	.055	O
26			.0009						.181	.045	O
27			.0017	.361	.361			.09	.251	.064	O
28			.0014						.207	.051	O
29			.0012						.177	.044	O
30			.0011						.162	.043	X
31			.0015	.441	.441			.11	.181	.046	O
32			.0013						.157	.039	X
33			.0017	.522	.522			.13	.176	.044	O
34			.0016						.168	.042	X
35	.500	2.00	.0020	.522	.522	.250	.250	.13	.208	.052	O
36			.0022						.220	.055	O
37	.833	2.00	.0015	.281	.281	.150	.417	.07	.171	.071	X
38			.0027						.307	.129	O
39			.0022						.250	.105	X
40			.0026						.296	.123	X
41			.0033						.376	.156	O
42			.0030	.361	.361				.266	.112	X

Table A3 - continued

Exp. No.	B	W	Q_i	Q_w	V_n	L/B	B/W	F_r	C_g	C	
	ft	ft	cfs	cfs	fps						
43			.0039						.346	.146	O
44			.0033						.293	.122	O
45			.0038	.441	.441			.11	.276	.115	X
46			.0049						.356	.149	O
47			.0047						.341	.142	O
48			.0048	.522	.522			.13	.294	.123	O
49			.0052						.321	.134	X
50			.0061						.372	.155	X
51			.0063						.388	.162	O
52	1.333	.200	.0054	.281	.281	.093	.667	.07	.387	.258	X
53			.0092						.658	.439	X
54			.0115						.822	.548	X
55			.0158						1.123	.749	X

Table A4 - Ice Jam Initiation Experiments with Large Plastic Blocks
(3 in x 2.5 in x 3/8 in)

Exp. No.	B	W	Q_i	Q_w	V_n	L/B	B/W	F_r	C_g	C	
	ft	ft	cfs	cfs	fps						
PF56	.833	2.00	.0021	.336	.336	.300	.417	.083	.206	.086	O
57			.0011						.110	.046	X
58			.0015						.144	.060	X
59			.0019						.185	.077	X
60			.0020						.194	.081	O
61			.0027	.386	.386			.095	.223	.093	O
62			.0024						.204	.085	O
63			.0024						.204	.085	X
64			.0024						.204	.085	X
65			.0029						.242	.101	O
66			.0033	.447	.447			.110	.240	.100	O
67			.0030						.213	.089	O
68			.0032						.233	.097	O
69			.0029						.206	.086	O
70			.0027						.197	.082	X
71			.0026						.187	.078	X
72			.0030						.221	.092	O
73			.0034	.487	.487			.120	.225	.094	O
74			.0032						.211	.088	O
75			.0035	.528	.528			.130	.213	.089	O
76			.0034						.206	.086	O
77			.0023						.141	.059	O
78			.0016						.096	.040	X
79			.0020						.120	.050	X
80			.0021						.125	.052	X
81			.0028						.168	.070	X
82			.0029						.175	.073	X
83			.0034						.206	.086	O
84			.0036	.573	.573			.140	.206	.086	O

Table A4 - continued

Exp. No.	B	W	Q_i	Q_w	V_n	L/B	B/W	F_r	C_g	C	
	ft	ft	cfs	cfs	fps						
85			.0037						.213	.089	X
86			.0035						.197	.082	O
87			.0036						.204	.085	X
88			.0041						.235	.098	X
89			.0042						.240	.100	X
90	.833	2.00	.0048	.573	.573	.300	.417	.140	.273	.114	O
91			.0046						.261	.109	O
92			.0069	.614	.614			.150	.364	.152	O
93			.0078						.410	.171	O
94			.0102	.642	.642			.160	.506	.211	O
95			.0061						.086	.036	X
96			.0096						.479	.200	X
97			.0119						.595	.248	X
98			.0130						.647	.270	O
99			.0089						.443	.185	O
100			.0074						.372	.155	O
101			.0186	.780	.780			.194	.762	.318	X
102	1.333	2.00	.0046	.361	.361	.187	.667	.090	.255	.170	X
103			.0077						.428	.285	O
104			.0076						.418	.279	O
105			.0058						.324	.216	X
106			.0066						.366	.244	X
107			.0081	.441	.441			.110	.369	.246	X
108			.0110						.498	.332	O
109			.0094						.427	.285	O
110			.0098						.448	.299	O
111			.0084						.382	.255	O
112			.0128	.481	.481			.120	.531	.354	O

Table A4 - continued

Exp. No.	B	W	Q_i	Q_w	V_n	L/B	B/W	F_r	C_g	C	
	ft	ft	cfs	cfs	fps						
113			.0094						.388	.259	O
114			.0099						.414	.276	X
115			.0092						.381	.254	O
116			.0088						.367	.245	X
117			.0131	.522	.522			.130	.502	.335	O
118			.0104						.397	.265	O
119			.0113						.432	.288	X
120			.0108						.414	.276	O
121			.0101						.387	.258	O
122			.0094						.360	.240	X
123			.0195	.562	.562			.140	.694	.463	O
124	1.333	2.00	.0116	.562	.562	.187	.667	.140	.414	.276	O
125			.0113						.402	.268	X
126			.0108						.382	.255	X
127			.0119	.642	.642			.160	.370	.247	X
128			.0154						.481	.321	X
129			.0193						.601	.401	O
130			.0220	.722	.722			.180	.610	.407	X
131	.667	2.00	.0008	.361	.361	.375	.333	.090	.093	.031	O
132			.0010						.111	.037	X
133			.0008						.096	.032	X
134			.0012						.138	.046	O
135			.0012						.138	.046	O
136			.0022	.441	.441			.110	.195	.065	O
137			.0014						.126	.042	X
138			.0018						.165	.055	O
139			.0015						.138	.046	O
140			.0013						.123	.041	X

Table A4 - continued

Exp. No.	B	W	Q_i	Q_w	V_n	L/B	B/W	F_r	C_g	C	
	ft	ft	cfs	cfs	fps						
141			.0018	.522	.522			.130	.138	.046	O
142			.0016						.120	.040	X
143			.0015						.117	.039	X
144			.0021						.112	.054	O
145			.0017	.562	.562			.140	.126	.042	X
146			.0026						.183	.061	X
147			.0043						.309	.103	O
148			.0032						.225	.075	O
149			.0031						.219	.073	O
150			.0021						.144	.048	X
151			.0032	.602	.602			.150	.216	.072	X
152			.0054						.363	.121	O
153			.0050						.330	.110	O
154			.0035						.234	.078	X
155			.0109	.682	.682			.170	.639	.213	X
156			.0161						.942	.314	X

Table A5 - Ice Jam Initiation Experiments with Paraffin Blocks
(1 3/4 in x 1 3/4 in x ½ in)

Exp. No.	B	W	Q_i	Q_w	V_n	L/B	B/W	F_r	C_g	C	
	ft	ft	cfs	cfs	fps						
PA1	.667	2.00	.0033	.241	.241	.219	.333	.060	.411	.137	O
2			.0018						.228	.076	X
3			.0024						.303	.101	O
4			.0021						.261	.087	O
5			.0018						.222	.074	O
6			.0012						.147	.049	X
7			.0014						.174	.058	X
8			.0033	.321	.321			.080	.306	.102	O
9			.0019						.180	.060	X
10			.0025						.231	.077	X
11			.0028						.267	.089	O
12			.0041	.401	.401			.100	.306	.103	O
13			.0033						.246	.082	X
14			.0036						.267	.089	O
15			.0032						.237	.079	X
16	.833	2.00	.0027	.241	.241	.175	.417	.060	.339	.113	X
17			.0031						.387	.129	X
18			.0041						.519	.173	O
19			.0036						.453	.151	O
20			.0058	.321	.321			.080	.540	.180	O
21			.0045						.417	.139	O
22			.0029						.276	.092	X
23			.0035						.324	.108	X
24			.0040						.378	.126	X

APPENDIX B

Experimental Results for Ice Jam Thickness Study

Table B1 - Equilibrium Jam Thickness - Experiments with Small Ice Floes (1½ in x 1¼ in x 5/16 in) ($\rho'/\rho = 0.92$, $F_C = 0.58$)

Exp. No.	h_n (ft)	V_n (cfs)	C	t_e (ft)	F_r	$\frac{t_e}{h_n}$	$\frac{\rho'}{\rho}\frac{t_e}{t_i} - 1$	F_D	$F_D - F_C$
SI1	.31	.41	.13	.144	.13	.46	4.09	3.53	2.95
2	.31	.41	.28	.114	.13	.36	3.04	2.69	2.11
3	.31	.41	.91	.068	.13	.22	1.39	1.79	1.21
4	.31	.41	.65	.096	.13	.31	2.39	2.24	1.66
5	.31	.28	.71	.055	.09	.18	0.96	0.81	0.23
6	.32	.27	.14	.045	.09	.14	0.59	0.68	0.10
7	.33	.35	.17	.058	.11	.18	1.07	1.24	0.66
8	.33	.35	.86	.055	.11	.17	0.95	1.21	0.63
9	.51	.59	.10	.232	.15	.46	7.22	7.05	6.47
10	.51	.59	.25	.197	.15	.39	5.96	5.74	5.16
11	.51	.59	.24	.216	.15	.42	6.64	6.39	5.81
12	.51	.59	.62	.187	.15	.37	5.96	5.42	4.84
13	.50	.52	.11	.182	.13	.37	5.46	4.18	3.60
14	.50	.52	.15	.182	.13	.36	5.44	4.13	3.55
15	.51	.52	.19	.177	.13	.35	5.27	4.00	3.42
16	.51	.52	.24	.165	.13	.33	4.84	3.76	3.18
17	.49	.52	.29	.187	.13	.38	5.61	4.37	3.79
18	.49	.52	.37	.171	.13	.35	5.04	4.01	3.43
19	.49	.52	.57	.142	.13	.29	4.00	3.45	2.87
20	.49	.52	.80	.151	.13	.31	4.34	3.61	3.03
21	.50	.61	.10	.197	.15	.39	5.96	6.21	5.63
22	.50	.44	.13	.142	.11	.28	4.03	2.46	1.88
23	.50	.44	.34	.133	.11	.27	3.69	2.35	1.77
24	.50	.44	.68	.115	.11	.23	3.07	2.16	1.58
25	.50	.44	.95	.146	.11	.29	4.16	2.50	1.92
26	.71	.62	.09	.213	.13	.30	6.52	5.11	4.53
27	.71	.62	.35	.203	.13	.29	6.19	4.94	4.36
28	.71	.62	.72	.204	.13	.29	6.22	4.96	4.38

Table B1 - continued

Exp. No.	h_n (ft)	V_n (cfs)	C	t_e (ft)	F_r	$\frac{t_e}{h_n}$	$\frac{\rho'}{\rho}\frac{t_e}{t_i} - 1$	F_D	$F_D - F_C$
29	.71	.53	.13	.180	.11	.25	5.36	3.30	2.72
30	.71	.53	.65	.123	.11	.17	3.36	2.76	2.18
31	.71	.53	.95	.138	.11	.20	3.89	2.89	2.31
32	.72	.43	.16	.108	.09	.15	2.80	1.78	1.20
33	.72	.43	.57	.074	.09	.10	1.62	1.61	1.03

Table B2 - Equilibrium Jam Thickness - Experiments with Large Ice Floes (3 in x 2.5 in x 5/16 in) ($\rho'/\rho = 0.92$, $F_C = 0.58$)

Exp. No.	h_n (ft)	V_n (cfs)	C	t_e (ft)	F_r	$\frac{t_e}{h_n}$	$\frac{\rho'}{\rho}\frac{t_e}{t_i} - 1$	F_D	$F_D - F_C$
LI1	.52	.47	.20	.175	.11	.34	5.20	3.29	2.71
2	.52	.47	.60	.128	.11	.25	3.54	2.62	2.04
3	.52	.47	.92	.111	.11	.22	2.94	2.43	1.85
4	.52	.47	1.17	.086	.11	.17	2.05	2.19	1.61
5	.51	.39	.25	.075	.10	.15	1.65	1.45	0.87
6	.51	.39	.58	.065	.10	.13	1.30	1.40	0.82
7	.51	.39	.72	.058	.10	.11	1.04	1.36	0.78
8	.51	.39	1.03	.049	.10	.10	0.73	1.30	0.72
9	.50	.53	.20	.169	.13	.31	4.97	4.09	3.51
10	.50	.53	.49	.164	.13	.30	4.81	4.00	3.42
11	.50	.53	.77	.084	.13	.15	1.96	2.73	2.15
12	.50	.53	.99	.082	.13	.15	1.91	2.71	2.13
13	.70	.62	.17	.303	.13	.43	9.74	7.22	6.64
14	.70	.62	.46	.266	.13	.38	8.40	6.19	3.69
15	.70	.62	.74	.186	.13	.26	5.59	4.62	4.04
16	.70	.62	.99	.188	.13	.27	5.66	4.66	4.08
17	.71	.55	.18	.292	.11	.41	9.31	5.31	4.73
18	.71	.55	.51	.172	.11	.24	5.09	3.43	2.85
19	.71	.55	.74	.174	.11	.25	5.15	3.44	2.86
20	.71	.55	1.11	.158	.11	.22	4.59	3.28	2.70
21	.71	.49	.20	.162	.10	.23	4.75	2.66	2.08
22	.71	.49	.54	.125	.10	.18	3.43	2.37	1.79
23	.71	.49	.90	.102	.10	.14	2.61	2.20	1.62
24	.71	.49	1.26	.111	.10	.16	2.94	2.26	1.68

Table B3 - Equilibrium Jam Thickness - Experiments with Small Plastic Blocks (1½ in x 1¼ in x 3/8 in) ($\rho'/\rho = 0.91$, $F_C = 1.22$)

Exp. No.	h_n (ft)	V_n (cfs)	C	t_e (ft)	F_r	$\frac{t_e}{h_n}$	$\frac{\rho'}{\rho}\frac{t_e}{t_i} - 1$	F_D	$F_D - F_C$
SP1	.31	.47	.14	.044	.15	.14	0.28	1.43	0.21
2	.31	.47	.67	.035	.15	.12	0.03	1.35	0.13
3	.31	.47	1.45	.135	.15	.44	2.92	2.96	1.74
4	.50	.61	.13	.094	.15	.19	1.73	2.59	1.37
5	.50	.61	.58	.076	.15	.15	1.22	1.83	0.61
6	.50	.61	1.23	.130	.15	.26	2.79	3.05	1.83
7	.51	.66	.11	.142	.16	.28	3.14	3.80	2.58
8	.51	.66	.63	.075	.16	.15	1.17	2.83	1.61
9	.51	.66	1.26	.126	.16	.25	2.68	3.53	2.31
10	.50	.52	.13	.055	.13	.11	0.61	1.64	0.42
11	.50	.52	.58	.048	.13	.10	0.40	1.59	0.37
12	.50	.52	1.30	.115	.13	.23	2.36	2.12	0.90
13	.69	.71	.10	.124	.15	.18	2.60	3.44	2.22
14	.69	.71	.55	.085	.15	.12	1.47	3.06	1.84
15	.69	.71	1.26	.196	.15	.28	4.70	4.35	3.13
16	.69	.61	.12	.074	.13	.11	1.15	2.25	1.03
17	.69	.61	.57	.074	.13	.11	1.16	2.25	1.03
18	.69	.61	1.17	.133	.13	.19	2.88	2.69	1.47
19	.70	.52	.11	.051	.11	.07	0.48	1.53	0.31
20	.70	.52	.54	.048	.11	.07	0.40	1.52	0.30
21	.70	.52	1.41	.132	.11	.19	2.85	1.94	0.72

AD-A032 471 IOWA INST OF HYDRAULIC RESEARCH IOWA CITY F/G 13/2
A LABORATORY INVESTIGATION OF THE MECHANICS AND HYDRAULICS OF R--ETC(U)
MAR 76 J C TATINCLAUX, C L LEE, T P WANG DAAK03-75-C-0030
UNCLASSIFIED IIHR-186 NL

2 OF 2
AD-A
032 471

END
DATE
FILMED
1-28-77
NTIS

Table B4 - Equilibrium Jam Thickness - Experiments with Large Plastic Blocks (3 in x 2.5 in x 3/8 in) ($\rho'/\rho = 0.91$, $F_C = 1.22$)

Exp. No.	h_n (ft)	V_n (cfs)	C	t_e (ft)	Fr	$\frac{t_e}{h_n}$	$\frac{\rho'}{\rho}\frac{t_e}{t_i} - 1$	F_D	$F_D - F_C$
LP1	.31	.46	.13	.064	.15	.21	.87	1.53	0.31
2	.31	.46	.57	.052	.15	.17	.51	1.41	0.19
3	.31	.46	1.42	.040	.15	.13	.16	1.29	0.07
4	.50	.60	.17	.120	.15	.24	2.49	2.84	1.62
5	.50	.60	.60	.130	.15	.26	2.79	2.97	1.75
6	.50	.60	1.09	.132	.15	.26	2.83	3.00	1.78
7	.50	.60	1.19	.116	.15	.24	2.39	2.79	1.57
8	.50	.51	.08	.107	.13	.21	2.10	1.98	0.76
9	.50	.51	.63	.059	.13	.11	0.73	1.60	0.38
10	.50	.51	1.21	.107	.13	.22	2.12	1.99	0.77
11	.50	.49	.10	.069	.11	.14	1.01	1.54	0.32
12	.50	.49	.60	.073	.11	.15	1.12	1.57	0.35
13	.50	.49	1.41	.149	.11	.30	3.33	2.21	0.99
14	.71	.71	.47	.208	.15	.29	5.04	4.50	3.28
15	.71	.71	1.18	.206	.15	.29	5.01	4.48	3.26
16	.71	.61	.07	.144	.13	.20	3.20	2.69	1.47
17	.71	.61	.62	.083	.13	.12	1.40	2.23	1.01
18	.71	.61	1.24	.113	.13	.16	2.29	2.45	1.23
19	.69	.61	.10	.074	.13	.11	1.16	2.25	1.03
20	.69	.61	.32	.058	.13	.08	0.67	2.15	0.93
21	.69	.61	.91	.071	.13	.10	1.07	2.24	1.02
22	.70	.53	.12	.067	.11	.10	0.94	1.63	0.41
23	.70	.53	.65	.075	.11	.11	1.17	1.67	0.45
24	.70	.53	1.36	.161	.11	.23	3.70	2.18	0.96

APPENDIX C

Effect of Surface Tension on Submergence Velocity of Ice Blocks

In the course of the study of ice jam initiation and development the velocities for incipient submergence of the plastic blocks were measured and found to be forty to fifty percent higher than that for ice blocks of nearly identical thickness. Since the specific mass of the polyethylene is nearly equal to that of fresh-water ice (0.91 as compared to 0.92 for ice), all of the formulas proposed in the literature for computing the critical submergence velocity would predict nearly the same value of the critical submergence velocity for both the ice blocks and the plastic blocks used in the present study. For example, Ashton's (1974) formula

$$\frac{V_c}{[gt_i(1-\frac{\rho'}{\rho})]^{\frac{1}{2}}} = \frac{2(1-t_i/h_n)}{[5-3(1-t_i/h_n)^2]^{\frac{1}{2}}} \qquad \text{(A1)}$$

predicts for a depth h_n of flow of 0.5 feet:
V_c = 0.32 fps for ice blocks (t_i = 0.026 ft, ρ' = 1.785 slug/ft^3), and
V_c = 0.37 fps for plastic blocks (t_i = 0.031 ft, ρ' = 1.765 slug/ft^3)
while the measured values of V_c were 0.32 to 0.36 fps and 0.44 to 0.48 fps, respectively. The measured value is correctly predicted by the theory for ice blocks, but it is some thirty percent higher than the theoretical one for plastic blocks.

Polyethylene is a non-wetting material; therefore, along the sides of a floating block, the water meniscus is convex upward. As a result, at a flow velocity nearly equal to the critical submergence velocity, the edge of the block is slightly below the water surface as is shown by figure 23 and is depicted in figure 24. The water surface displacement δ due to this surface tension effect can be calculated theoretically when the surface tension factor c at the air-water interfaces is known as

$$\delta^2 = \frac{2c}{\rho g}\,(1 - \sin\theta) \qquad \text{(A2)}$$

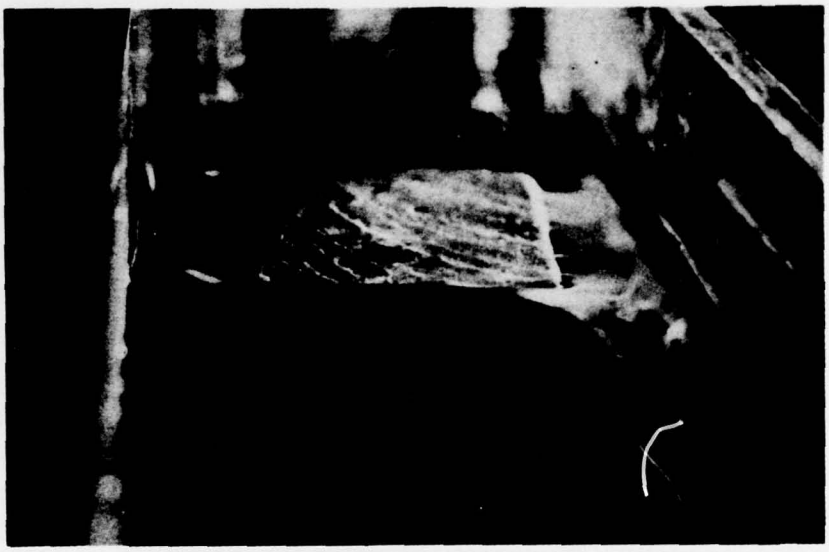

Figure 23. Photograph of Polyethylene Block in a Stream Showing Effect of Surface Tension

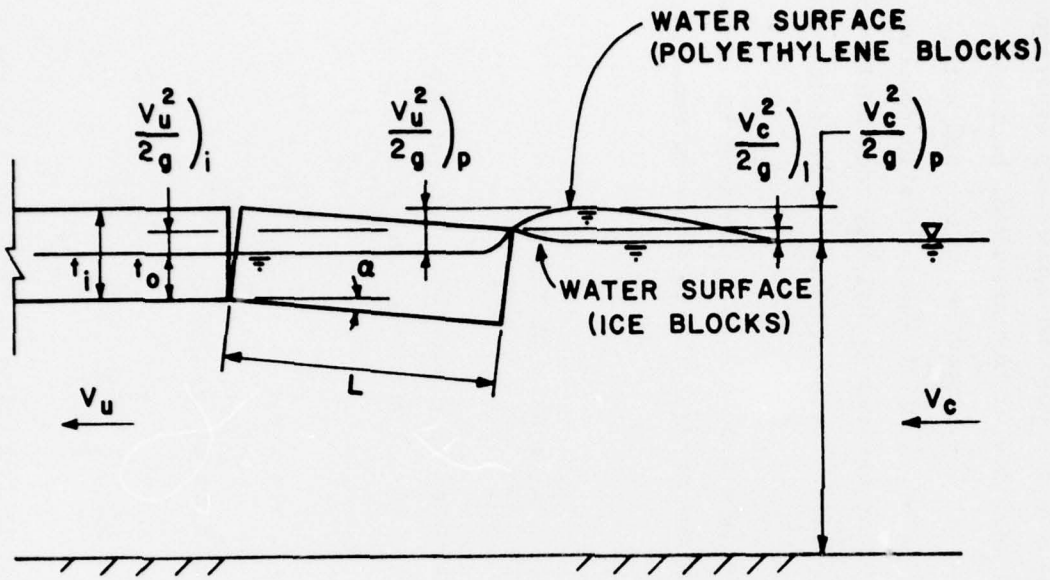

Figure 24. Definition Sketch for Determination of Submergence Velocity Including Surface Tension Effects

and θ is the contact angle at the air-water-plastic interface, and was calculated by Wu (1971) to be 102°. Taking c equal to 76 dynes/cm the corresponding value of δ is calculated as 0.06 cm.

The effect of surface tension has been recognized by B. Michel (1957), who had incorporated it in his analysis. He pointed out that the effect of surface tension can become very significant when small blocks of material other than ice are used in laboratory experiments to simulate ice floes. When real ice blocks are used, because of the film of water which is present at the interface of ice and water, this surface tension effect is not present or at least greatly reduced. This writer is not aware of any author besides Michel who took surface tension into consideration in his analysis for the determination of the critical submergence velocity.

Ashton's (1974) analysis can be easily modified to include surface tension effects. His moment-equilibrium analysis remains valid and leads to the equation

$$\frac{V_u^2}{2gt_i} - \frac{V_u^2}{2gt_i} = -\frac{\rho'}{\rho} + \frac{t_o}{t_i} + \frac{2L \sin \alpha}{3t_i} \qquad \text{(A3)}$$

where the various terms are defined in Figure 24. The surface tension effect is introduced into the no-spill condition for stability of the block, which becomes

$$t_o + \frac{V_c^2}{2g} + L \sin \alpha = t_i + \delta \qquad \text{(A4)}$$

Substituting for L sin α in A3 from A4 results in

$$\frac{5V_u^2}{6gt_i} - \frac{V_c^2}{2gt_i} = -\frac{\rho'}{\rho} + \frac{2}{3} + \frac{t_o}{3t_i} + \frac{2\delta}{3t_i}$$

The assumption $t_o = t_i\rho'/\rho$ and introduction of continuity by the relationship

$$V_c = V_u(1 - t_i/h_n)$$

lead to

$$\frac{V_c}{\sqrt{gt_i}} = \frac{2(1-t_i/h_n)}{[5-3(1-t_i/h_n)^2]^{\frac{1}{2}}} \sqrt{1-\frac{\rho'}{\rho}+\frac{\delta}{t_i}} \qquad \text{(A5)}$$

($\delta > 0$ for non wetting material and <0 for a wetting material)

If the value of δ calculated above is used in the computations, the critical submergence velocity for the polyethylene blocks used in the present experiments is found to be

$$V_c = 0.48 \text{ fps}$$

This result is very close to the experimentally measured values of 0.44 to 0.48 fps.

As can be seen from A5, the effect of surface tension becomes important when very small scale blocks, and therefore very thin blocks, are used in model studies to simulate real ice floes, and can lead to misleading results if the submergence velocity of the ice floes is an important parameter in the phenomenon under investigation.

The effect of surface tension was further confirmed by the following experiment. Polyethylene parallelepipeds were immersed in a chemical "cleaning" solution composed of 5 mg of sodium dychromate dissolved in 5 ml of water per 100 ml of concentrated H_2SO_4, and heated to a temperature of 60°C to 70°C. The resulting surface oxydation of the polyethylene modified its chemical composition and the material became wetting instead of nonwetting. The critical submergence velocity of the treated blocks was measured to be equal to 0.33 to 0.35 fps, similar to that of the real ice blocks and close to that predicted by A1. The oxidized film on the surface of the plastic block is very fragile and rubs off very easily. It was therefore impossible to perform the experiments on equilibrium jam thickness and ice jam initiation with oxidized plastic floes and determine whether the results would have been significantly altered and become similar to those obtained with ice floes.

In conclusion, when a phenomenon, in which the critical submergence velocity is an important parameter, is to be investigated in a model study and the ice floes are to be modeled using an artificial material, the scale of the model should be large enough to render the effects of

surface tension negligible, or, if no other considerations intervene, the thickness of the model floes should be adjusted such that their submergence velocity, including surface tension effect, is properly scaled.

APPENDIX D

Experimental Results on Compressive Strength of Fragmented Ice Cover

Table D1 - Summary of Compression Tests
($d \times b \times t_i$ = 1.378 in. x 1.378 in. x 1.378 in.)

Test No.	L (ft)	t (ft)	V_c (cm/s)	V_c/L (1/sec) x 10^{-4}	σ_{cr} (lbs/ft^2)	T_c (sec)
PG-1	3.0	0.3	0.037	4.0	52.39	Missing
PG-3	2.0	0.3	0.037	6.1	65.82	"
PG-4	2.0	0.3	0.043	7.1	50.15	"
PG-5	1.5	0.3	0.037	8.2	53.29	"
PG-6	1.5	0.3	0.043	9.6	43.88	"
PG-7	1.0	0.3	0.010	F >	200 lbs	"
PG-8	1.0	0.3	0.020	6.6	128.07	"
PG-9	1.0	0.3	0.040	13.1	64.48	"
PG-10	1.0	0.3	0.060	19.7	41.64	"
PG-11	1.0	0.3	0.080	16.1	31.79	"
PG-12	1.0	0.3	0.100	32.8	25.79	"
PG-13	2.0	0.3	0.010	1.6	168.81	"
PG-14	2.0	0.3	0.020	3.3	127.17	"
PG-15	2.0	0.3	0.040	6.6	51.05	"
PG-16	2.0	0.3	0.060	9.8	39.85	"
PG-17	2.0	0.3	0.080	13.1	30.45	"
PG-18	2.0	0.3	0.100	16.4	21.05	"
PG-19	3.0	0.3	0.010	F >	200 lbs	"
PG-20	3.0	0.3	0.020	2.2	128.96	"
PG-21	3.0	0.3	0.040	4.4	64.03	"
PG-22	3.0	0.3	0.060	6.6	40.75	"
PG-23	3.0	0.3	0.080	8.7	31.79	"
PG-24	3.0	0.3	0.100	10.9	21.94	"

Table D2 - Summary of Compression Tests
($d \times b \times t_i$ = 1.50 in. x 1.25 in. x 0.313 in.)

Test No.	L (ft)	t (ft)	V_c (cm/s)	V_c/L (1/sec) x 10^{-4}	σ_{cr} (lbs/ft^2)	T_c (sec)
KN-1	3.6	0.2	0.020	F >	200 lbs	
KN-2	3.6	0.2	0.040	3.7	52.80	59.8
KN-3	3.6	0.2	0.070	6.4	55.17	Missing
KN-4	3.6	0.2	0.090	8.2	31.58	25.2
KN-5	3.6	0.2	0.150	13.7	11.88	8.6
KN-6	3.6	0.2	0.200	18.2	10.04	6.8
KN-7	2.6	0.4	0.030	F >	200 lbs	
KN-8	2.6	0.4	0.054	6.8	47.56	40.0
KN-9	2.6	0.4	0.084	10.6	36.64	26.2
KN-10	2.6	0.4	0.120	15.1	22.62	16.8
KN-11	2.6	0.4	0.180	22.7	15.41	10.0
KN-12	3.0	0.4	0.030	3.3	99.55	110.2
KN-13	3.0	0.4	0.065	7.1	26.30	28.6
KN-14	3.0	0.4	0.095	10.4	20.13	18.0
KN-15	3.0	0.4	0.140	15.3	14.48	10.6
KN-16	3.0	0.4	0.190	20.7	12.51	7.3
KN-17	2.0	0.2	0.035	5.8	72.97	49.6
KN-18	2.0	0.2	0.052	8.5	43.61	31.2
KN-19	2.0	0.2	0.078	12.8	23.80	15.1
KN-20	2.0	0.2	0.130	21.3	12.85	7.0
KN-21	2.0	0.2	0.170	27.4	10.73	6.2
KN-31	2.0	0.6	0.200	32.8	22.90	8.8
KN-32	2.0	0.6	0.160	26.2	26.74	10.2
KN-33	2.0	0.6	0.110	18.1	54.16	20.9
KN-34	2.0	0.6	0.076	F >	200 lbs	

Table D2 - continued

Test No.	L (ft)	t (ft)	V_c (cm/s)	V_c/L (1/sec) x 10^{-4}	σ_{cr} (lbs/ft^2)	T_c (sec)
KN-37	6.0	0.2	0.18	9.8	7.95	9.8
KN-38	6.0	0.2	0.13	7.1	11.35	16.1
KN-39	6.0	0.2	0.10	5.5	15.81	25.7
KN-40	6.0	0.2	0.08	4.4	29.83	43.6
KN-41	6.0	0.2	0.06	3.3	28.08	55.3
KN-42	6.0	0.2	0.03	1.6	48.48	117.6
KN-43	6.0	0.2	0.02	1.1	62.73	159.7

Table D3 - Summary of Compression Tests
($d \times b \times t_i$ = 3 in. x 2.5 in. x 0.375 in.)

Test No.	L (ft)	t (ft)	V_c (cm/s)	V_c/L (1/sec) x 10^{-4}	σ_{cr} (lbs/ft^2)	T_c (sec)
KN-44	2.0	0.2	0.200	32.8	15.98	41.1
KN-45	2.0	0.2	0.150	24.6	13.89	23.4
KN-46	2.0	0.2	0.115	18.9	16.27	33.4
KN-47	2.0	0.2	0.070	11.5	15.89	15.1
KN-48	2.0	0.2	0.050	8.2	19.51	18.9
KN-49	2.0	0.2	0.038	6.2	22.55	24.1
KN-50	2.0	0.2	0.025	4.1	32.54	38.8
KN-51	3.0	0.2	0.190	20.8	16.08	16.2
KN-52	3.0	0.2	0.140	15.3	15.80	8.1
KN-53	3.0	0.2	0.110	12.0	18.55	8.7
KN-54	3.0	0.2	0.075	8.2	26.64	14.7
KN-55	3.0	0.2	0.055	6.0	37.43	24.4
KN-56	3.0	0.2	0.035	3.8	64.11	46.4
KN-57	3.0	0.2	0.024	2.6	86.41	70.7
KN-58	2.0	0.4	0.190	31.2	11.98	13.1
KN-59	2.0	0.4	0.140	23.0	10.46	8.8
KN-60	2.0	0.4	0.110	18.1	13.51	11.2
KN-61	2.0	0.4	0.075	12.3	16.42	14.8
KN-62	2.0	0.4	0.055	9.0	20.36	17.4
KN-63	2.0	0.4	0.035	5.7	46.37	40.5
KN-64	2.0	0.4	0.024	3.9	54.15	46.6